

1 **A mutant form of Dmc1 that bypasses the requirement for accessory protein**
2 **Mei5-Sae3 reveals independent activities of Mei5-Sae3 and Rad51 in Dmc1**
3 **filament stability**

4
5 **Short Title:** A Dmc1 mutant that bypasses Mei5-Sae3

6
7 Diedre Reitz¹, Jennifer Grubb², Douglas K. Bishop^{1,2,*}

- 8
9 1. Committee on Genetics, Genomics, and Systems Biology, University of Chicago,
10 Chicago, Illinois, USA
11
12 2. Department of Radiation and Cellular Oncology, Department of Molecular
13 Genetics and Cell Biology, University of Chicago, Chicago, Illinois, USA

14
15 * Correspondence: dbishop@uchicago.edu

16 **Abstract**

17 During meiosis, homologous recombination repairs programmed DNA double-stranded breaks
18 (DSBs). Meiotic recombination physically links the homologous chromosomes (“homologs”), creating the
19 tension between them that is required for their segregation. The central recombinase in this process is
20 Dmc1. Dmc1’s activity is regulated by its accessory factors Mei5-Sae3 and Rad51. We use a gain-of-
21 function *dmc1* mutant, *dmc1-E157D*, that bypasses Mei5-Sae3 to gain insight into the role of this
22 accessory factor and its relationship to mitotic recombinase Rad51, which also functions as a Dmc1
23 accessory protein during meiosis. We find that Mei5-Sae3 has a role in filament formation and stability,
24 but not in the bias of recombination partner choice that favors homolog over sister chromatids. We also
25 provide evidence that Mei5-Sae3 promotes Dmc1 filament formation specifically on single-stranded DNA.
26 Analysis of meiotic recombination intermediates suggests that Mei5-Sae3 and Rad51 function
27 independently in promoting filament stability. In spite of its ability to load onto single-stranded DNA and
28 carry out recombination in the absence of Mei5-Sae3, recombination promoted by the Dmc1 mutant is
29 abnormal in that it forms foci in the absence of DNA breaks, displays unusually high levels of multi-
30 chromatid and intersister (IS) joint molecules intermediates, as well as high levels of ectopic
31 recombination products. We use super-resolution microscopy to show that the mutant protein forms
32 longer foci than those formed by wild-type Dmc1 (Dmc1-WT). Our data support a model in which longer
33 filaments are more prone to engage in aberrant recombination events, suggesting that filaments lengths
34 are normally limited by a regulatory mechanism that functions to prevent recombination-mediated
35 genome rearrangements.

36

37 **Author Summary**

38 During meiosis, two rounds of division follow a single round of DNA replication to create the
39 gametes for biparental reproduction. The first round of division requires that the homologous
40 chromosomes become physically linked to one another to create the tension that is necessary for their
41 segregation. This linkage is achieved through DNA recombination between the two homologous
42 chromosomes, followed by resolution of the recombination intermediate into a crossover (CO). Central to
43 this process is the meiosis-specific recombinase Dmc1, and its accessory factors, which provide

44 important regulatory functions to ensure that recombination is accurate, efficient, and occurs
45 predominantly between homologous chromosomes, and not sister chromatids. To gain insight into the
46 regulation of Dmc1 by its accessory factors, we mutated Dmc1 such that it was no longer dependent on
47 its accessory factor Mei5-Sae3. Our analysis reveals that Dmc1 accessory factors Mei5-Sae3 and Rad51
48 have independent roles in stabilizing Dmc1 filaments. Furthermore, we find that although Rad51 is
49 required for promoting recombination between homologous chromosomes, Mei5-Sae3 is not. Lastly, we
50 show that our Dmc1 mutant forms abnormally long filaments, and high levels of aberrant recombination
51 intermediates and products. These findings suggest that filaments are actively maintained at short lengths
52 to prevent deleterious genome rearrangements.

53

54 **Introduction**

55 Homologous recombination is a high-fidelity mechanism of repair of DNA double strand breaks
56 (DSBs), interstrand cross-links, and stalled or collapsed replication forks. In addition, during meiosis, most
57 eukaryotes rely on CO recombination to physically link the maternal and paternal chromosomes via
58 chiasmata, thereby making it possible for the meiosis I spindle to create the tension between homolog
59 pairs that is required for their reductional segregation [1]. The RecA homolog Dmc1 plays the central
60 catalytic role in meiotic recombination in budding yeast [2,3]. Following DSB formation and end resection,
61 Dmc1 forms a helical nucleoprotein filament on the single-stranded DNA (ssDNA) tracts created by the
62 resection machinery [4]. The nucleoprotein filament then searches the genome for a sequence of duplex
63 DNA that is homologous to the ssDNA onto which it is loaded [5]. This region of homology can be an
64 allelic site on one of the two homologous chromatids or on the sister chromatid. In addition, if a DSB is in
65 a region that is repeated at more than one chromosomal locus, this can result in ectopic recombination
66 between the two chromosomal loci [6-9]. Meiotic recombination normally favors the use of the
67 homologous chromosome rather than the sister, consistent with the biological requirement for
68 interhomolog (IH) COs for reductional segregation; this phenomenon is known as “IH bias” [10,11]. Once
69 a homologous tract of double-stranded DNA (dsDNA) is found, strand exchange occurs to form a tract of
70 hybrid DNA, pairing the ssDNA with the complementary strand of the duplex. Hybrid DNA formation

71 displaces the opposite strand of the donor dsDNA, forming a displacement loop (D-loop) [12]. The repair
72 process then uses the intact donor duplex DNA as a template to direct DNA repair synthesis.

73 Homologous recombination is highly regulated to ensure its accuracy and avoid potentially
74 deleterious consequences of the process. Two key steps in homologous recombination, nucleoprotein
75 filament formation and the initial invasion event, are reversible and therefore subject to this regulation
76 [13]. Nucleoprotein filament formation, or nucleation, involves recruitment of the strand exchange protein
77 to sites with tracts of ssDNA, nucleation of filament formation which involves displacement of the high
78 affinity ssDNA binding protein RPA, and filament elongation which is driven by cooperative interactions
79 between strand exchange protomers. A class of accessory proteins collectively referred to as “mediator”
80 proteins can act to promote the displacement of RPA for filament nucleation and/or to stabilize nascent
81 filaments, allowing them to elongate [14,15]. Mutants lacking one of these assembly proteins display
82 defects in formation of filaments on ssDNA that can be detected by immunostaining or other cytological
83 methods following DNA damaging treatment, or during the normal meiotic program. UvrD family
84 helicases, including UvrD in prokaryotes and Srs2 in budding yeast, antagonize recombination at this step
85 by disassembling ssDNA nucleoprotein filaments [16-19]. Though the strippase function of Srs2 with
86 respect to Rad51 filaments has been well documented, Srs2 does not disassemble Dmc1 filaments, and
87 in fact Dmc1 may inhibit Srs2 activity on ssDNA [20,21]. It is currently unknown whether there exists an
88 ssDNA “strippase” for Dmc1.

89 Under normal circumstances *in vivo*, RecA family proteins form nucleoprotein filaments that are
90 usually shorter than the resolution limit of conventional light microscopy (~200 nanometers). This is true
91 for RecA, and for both eukaryotic RecA homologs, Rad51 and Dmc1 [22-25]. Super-resolution
92 microscopy imaging of Dmc1 filaments formed during meiosis indicates that Dmc1 filaments are typically
93 about 120 nanometers long, a length that roughly corresponds to 100 nucleotides when taking into
94 account the fact that RecA family proteins stretch the DNA ~1.5 fold when assembled into a filament, and
95 the length added by antibody decoration [26,27]. Furthermore, in the *exo1-D173A* mutant, in which DNA
96 end resection is impaired during meiosis, joint molecules are formed at a level that is equivalent to wild-
97 type, implying that short ssDNA tracts support normal meiotic recombination [28]. In addition, longer than
98 normal Dmc1 filaments accumulate in the absence of Mnd1, a Dmc1 accessory protein that is required for

99 Dmc1 activity after the filament formation stage [26]. Taken together, these results suggest that while
100 RecA family proteins are competent to form long filaments, they are regulated such that they form
101 relatively short filaments *in vivo*, though the significance of this regulation and the factors that influence
102 filament length are not well understood.

103 RecA family recombinases are DNA-dependent ATPases, but their ATPase activity is not
104 required for filament formation or for strand exchange [29-32]. Instead, ATP binding changes the
105 conformation of the protein to a form that has high affinity for DNA, and is thus the active form [29,33].
106 The ADP bound form of the protein has lower affinity for DNA than the ATP-bound form, and is inactive in
107 homology search and strand exchange. In prokaryotes, RecA ATP hydrolysis is required for filament
108 disassembly following strand exchange, or when the protein inappropriately assembles on dsDNA
109 [25,32]. In contrast to RecA, the eukaryotic recombinases Rad51 and Dmc1 display relatively weak
110 intrinsic ATPase activity and rely on Rad54 family ATP-dependent dsDNA translocases to promote their
111 dissociation [34-38]. Translocase driven dissociation is required to clear strand exchange proteins from D-
112 loops to allow completion of recombination events [39]. Translocases also prevent accumulation of off-
113 pathway complexes formed by filament nucleation on unbroken dsDNA [37,39-43]. The translocases may
114 be of particular importance in eukaryotes because, unlike RecA, *in vitro* single-molecule fluorescence
115 imaging showed that Rad51-ADP dissociation from dsDNA is inefficient and incomplete, suggesting that
116 the activity of the translocases is required even when Rad51 is in the ADP-bound form [44]. Moreover,
117 Rad54 was observed to have an effect on Rad51-K191R, a Rad51 mutant that is completely defective in
118 ATP hydrolysis, implying that the ATPase activity of Rad51 is not required for it to be removed from
119 dsDNA by Rad54 [45-47]. Finally, in the context of the nucleoprotein filament, the ATPase domain of one
120 protomer directly contacts the N-terminal binding domain of the adjacent protomer; this observation is
121 believed to be the structural basis for the observation that ATP-binding promotes protomer-protomer
122 cooperativity [48,49].

123 We are interested in understanding how accessory proteins regulate the activity of the meiotic
124 RecA homolog Dmc1. In *Saccharomyces cerevisiae*, Dmc1's activity is regulated by at least five key
125 accessory proteins including RPA, Mei5-Sae3, Hop2-Mnd1, Rad51, and the translocase Rdh54 (a.k.a.
126 Tid1). RPA rapidly binds to tracks of ssDNA and serves to regulate interactions of Dmc1's other

127 accessory proteins with ssDNA [50]. *In vivo*, Mei5-Sae3 and Rad51 are required for normal Dmc1
128 filament formation at tracts of RPA coated ssDNA [51-53]. Hop2-Mnd1 is required for strand exchange,
129 but not for filament nucleation or stability [54,55]. Rdh54 is a Rad54 family translocase implicated in
130 promoting dissociation of Dmc1 from dsDNA, as discussed above.

131 Budding yeast Mei5-Sae3 is a homolog of *Schizosaccharomyces pombe* and mammalian Sfr1-
132 Swi5/MEI5-SWI5, with no known homolog in plants [56]. In budding yeast, Mei5-Sae3 is Dmc1-specific,
133 whereas in fission yeast Sfr1-Swi5 is an accessory factor to both Dmc1 and the mitotic eukaryotic RecA
134 homolog Rad51 [57]. In mammals, MEI5-SWI5 protein is reported to function with RAD51, but there is no
135 known interaction with DMC1, and an effort to detect DMC1 stimulatory activity *in vitro* yielded negative
136 results [58,59]. Biochemical studies have suggested several functions for Mei5-Sae3. First, studies using
137 fission yeast proteins have shown that Sfr1-Swi5 stimulates fission yeast Rad51, Rph51, and Dmc1 in
138 three-stranded DNA exchange reactions, and it helps Rph51 overcome the inhibitory effect of RPA [57].
139 Studies using purified budding yeast Mei5-Sae3 and Dmc1 similarly concluded that Mei5-Sae3 promotes
140 Dmc1 loading onto RPA-coated ssDNA, and that it enhances Dmc1-mediated D-loop formation when
141 used alone, or in combination with Rad51 [3,50,60]. Haruta et al. also reported that Sfr1-Swi5 enhances
142 Rph51's ATPase activity; this result was subsequently clarified by work from Su et al. using purified *Mus*
143 *musculus* proteins [57,59]. Su et al. showed that SWI5-MEI5 stimulates RAD51 by promoting ADP
144 release, the step in ATP hydrolysis that is believed to be the slowest and thus rate-limiting [59,61].
145 Enhancement of ADP release is thought to have a stabilizing effect on Rad51 filaments by maintaining
146 them in the ATP-bound state. In addition, later studies using a single-molecule fluorescence resonance
147 energy transfer, concluded that mouse SWI5-MEI5 promotes RAD51 nucleation by preventing
148 dissociation, effectively reducing the number of protomers required for a nucleation event from three to
149 two [62]. The same study also found that fission yeast Sfr1-Swi5 prevents Rhp51 disassembly,
150 suggesting a conserved role for this complex in stabilizing Rad51 filaments.

151 *In vivo*, *Saccharomyces cerevisiae* Dmc1 and Mei5-Sae3 are interdependent for focus formation,
152 and the foci formed by the two proteins co-localize with one another, and with other DSB-dependent
153 proteins such as Rad51 [52,53]. Moreover, Dmc1 and Mei5-Sae3 both depend on Rad51 for normal
154 meiotic focus formation; average focus staining intensity is lower in *rad51* mutants than in wild-type

155 [51,52]. Consistent with its requirement for Dmc1 focus formation, Mei5-Sae3 is required for Dmc1-
156 mediated recombination *in vivo*; DSBs form normally in *mei5* or *sae3* mutants, but these intermediates
157 are not converted to D-loops [52,53,63]. Fission yeast Rph51 differs from Dmc1 in its dependency on
158 Sfr1-Swi5; while loss of Sfr1-Swi5 reduces recombination, recombination is only eliminated when both
159 Sfr1-Swi5 and fission yeast Rad55-Rad57 homologs, Rph55-Rdp57, are deleted [64]. Similarly,
160 knockdown of MEI5-SWI5 in human cells impairs RAD51 focus formation in response to ionizing radiation
161 and also reduces recombination [58]. In contrast, deletion of mouse *Swi5* and *Sfr1* does not reduce the
162 level of recombination when assayed with a direct-repeat reporter construct, but it does make cells more
163 sensitive to DNA damaging agents that require homologous recombination to repair, including ionizing
164 radiation, camptothecin, and poly(ADP-ribose) polymerase (PARP) inhibitor [65]. It is not known whether
165 these differences in the requirement of SWI5-MEI5 by RAD51 in humans and mouse are due to
166 differences in the cell types used or true biological differences in the human and mouse RAD51
167 recombinases [58].

168 Rad51, the RecA homolog that catalyzes homology search and strand exchange during mitotic
169 recombination, is the second accessory protein that plays a role in forming normal Dmc1 filaments during
170 meiosis [51]. Although Rad51 is required for normal meiotic recombination, its strand exchange activity is
171 dispensable [3]. In fact, Rad51 strand exchange activity is inhibited during meiosis I by the meiosis-
172 specific protein Hed1 [66,67]. In the absence of Rad51, Dmc1 foci have reduced staining intensity,
173 suggesting that filaments are defective [51,68]. Recombination still occurs in *rad51* mutants, but it is mis-
174 regulated such that D-loop formation occurs predominantly between sister chromatids, instead of
175 between homologous chromosomes [69]. In addition, CO formation is reduced, only a sub-population
176 progresses through meiotic divisions, and the spores formed are not viable [70]. In biochemical
177 reconstitution experiments, Rad51 alone can stimulate Dmc1-mediated D-loop formation, although
178 optimal levels of D-loop formation require both Rad51 and Mei5-Sae3 [3]. In spite of its importance as a
179 Dmc1 accessory factor, very little is known about the molecular mechanisms involved in Rad51's non-
180 catalytic role in meiotic recombination. In particular, it is not known if the role of Rad51 in homolog bias is
181 a consequence of its role in promoting Dmc1 filament formation.

182 One approach to studying the role of accessory proteins is to assume that the activity of the
183 enzyme has evolved to depend on that accessory factor. In this view, beneficial regulation of an enzyme's
184 activity is selected for at the expense of the enzyme's intrinsic activity. If such an evolutionary process is
185 responsible for a particular regulatory mechanism, it should be possible to mutate the core enzyme to
186 eliminate the "built-in" defect, rendering the mutant protein capable of catalyzing its reaction in the
187 absence of the accessory protein. Comparison of the activities of the mutant and wild-type proteins with
188 and without the accessory protein can then provide mechanistic insight into the processes that accessory
189 protein normally regulates.

190 We applied this approach to Dmc1 in an attempt to further elucidate the mechanisms through
191 which Mei5-Sae3 influence's Dmc1 activity. We identified a gain-of-function Dmc1 mutant whose activity
192 is independent of Mei5-Sae3. Characterization of this Dmc1 mutant provides new insight into the
193 mechanism of action of Mei5-Sae3 *in vivo*, and also sheds light on the functional relationship between
194 Mei5-Sae3 and Rad51. Furthermore, characterization of this gain-of-function version of Dmc1 reveals that
195 it forms longer than normal filaments and displays higher than normal levels of IS, ectopic, and multi-
196 chromatid recombination. We interpret these observations in the context of recent studies showing that a
197 single strand exchange filament can simultaneously engage more than one dsDNA molecule.

198

199 **Results**

200 In order to better understand the function of Mei5-Sae3 and Rad51 in Dmc1-mediated HR, we
201 sought to identify a *DMC1* allele that would bypass the requirement for one of these accessory factors.
202 Analysis of Dmc1-mediated recombination in the absence of an accessory factor would then allow us to
203 identify regulatory features that depend on the accessory protein by comparison to the wild-type process.
204 To this end, we constructed two *dmc1* mutants based on two previously characterized gain-of-function
205 mutations in Dmc1 homologs, RecA-E96D and Rad51-I345T [32,71,72]. Sequence alignments indicated
206 that the amino acid residues altered in these mutants are conserved allowing us to construct
207 corresponding mutant forms of Dmc1; for RecA-E96D the corresponding mutant is Dmc1-E157D and for
208 Rad51-I134T the corresponding mutant is Dmc1-I282T.

209 To assess whether either of these Dmc1 mutants would bypass Mei5-Sae3 and/or Rad51, we
210 constructed diploid yeast lacking either Mei5 or Rad51 with the corresponding Dmc1 mutation, and
211 assessed sporulation efficiency and spore viability alongside *DMC1⁺ mei5* and *DMC1⁺ rad51* controls. In
212 a *mei5* strain, tetrads are formed very inefficiently, whereas in a *rad51* mutant, tetrads are formed, but
213 almost all spores within them are dead [52,53,70]. We found that *dmc1-E157D* bypasses Mei5-Sae3 with
214 respect to sporulation and spore viability (Table 1). The spore viabilities of *dmc1-E157D*, *dmc1-E157D*
215 *mei5*, and *dmc1-E157D sae3* are nearly identical to one another (57.6%, 50.3%, and 57.0% respectively),
216 suggesting that Dmc1-E157D function is largely independent of Mei5-Sae3. In contrast, *dmc1-E157D*
217 does not bypass the requirement for *rad51* with respect to spore viability (0.0% in *rad51* versus 0.74% in
218 *dmc1-E157D rad51*).

219 Spore viability data from the *dmc1-E157D/DMC1* heterozygote and *dmc1-E157D/DMC1 mei5^Δ*
220 heterozygote strains suggests that Dmc1-E157D is co-dominant with wild-type Dmc1 in the presence of
221 Mei5 (85.6%), but fully dominant to wild-type Dmc1 in the absence of Mei5 (58.8% in *dmc1-E157D/DMC1*
222 *mei5^Δ* versus 50.3% in *dmc1-E157D mei5*). In contrast to *dmc1-E157D*, we did not detect phenotypic
223 suppression in *dmc1-I282T* mutants, either with respect to prophase arrest in a *mei5* mutant background,
224 or with respect to spore viability in a *rad51* background. Importantly, the Dmc1-E157D mutation does not
225 result in increased expression or stability of the protein as assayed by Western blotting of meiotic yeast
226 whole cell extracts, thus ruling out a trivial explanation for Dmc1-E157D's bypass of the *mei5* and *sae3*
227 mutations (Supplemental Figure 1).

228 **Dmc1-E157D forms meiotic immunostaining foci in the absence of Mei5 and Rad51**

229 We next performed immunofluorescence staining of spread meiotic nuclei to examine Dmc1
230 focus formation in the *dmc1-E157D* and *dmc1-E157D mei5* strains. As shown previously, meiotic Dmc1-
231 WT focus formation is severely defective in *mei5* mutant cells, but *dmc1-E157D* forms bright Dmc1 foci in
232 the *mei5* mutant background (Figures 1a,b) [52,53]. Notably, Dmc1 foci accumulate to higher levels and
233 persist for longer in *dmc1-E157D* and *dmc1-E157D mei5* when compared to wild-type.

234 One model suggests that Mei5-Sae3 and Rad51 cooperate to promote Dmc1 filament formation.
235 Because *dmc1-E157D* bypasses *mei5*, we reasoned that if this model is correct, *dmc1-E157D* might also
236 bypass the defect seen for formation of brightly-staining Dmc1 foci in *rad51* cells, even it does not

237 suppress the spore viability defect observed in these cells. To test this, we constructed *dmc1-E157D*
238 *rad51* and *dmc1-E157D mei5 rad51* strains, and looked for Dmc1 focus formation in spread meiotic
239 nuclei. In contrast to a *rad51* single mutant, in which Dmc1-WT staining intensity is reduced, the Dmc1
240 foci observed in *dmc1-E157D rad51* and *dmc1-E157D mei5 rad51* nuclei were brighter and more
241 numerous than those in wild-type (Figures 1c,d) [51,68]. We conclude that *dmc1-E157D* bypasses the
242 role of Rad51 with respect to forming brightly staining Dmc1 foci.

243 ***dmc1-E157D* forms immunostaining foci in the absence of DSBs**

244 Because the Dmc1-E157D mutant is modeled after RecA-E96D, which has been shown to form
245 foci on undamaged DNA, we wanted to ask whether the same was true of the corresponding Dmc1
246 mutant [25]. To determine whether any of the foci that we observed in the *dmc1-E157D* background
247 resulted from binding to chromosomes independent of DSBs, we introduced the *spo11* mutation into our
248 *dmc1-E157D* strains to block DSB formation. Spo11 is the catalytic subunit of a meiosis-specific complex
249 that induces DSBs at the outset of meiosis [73]. Immunostaining of spread meiotic nuclei for Dmc1 and
250 RPA revealed that in contrast to the *spo11* single mutant, which typically forms few if any Dmc1 foci,
251 nearly all *spo11 dmc1-E157D* nuclei contained numerous Dmc1 foci (Figures 1e,f) [41]. RPA serves as a
252 marker for DSB-associated tracts of ssDNA in mid-to-late prophase I. RPA foci are detected early in
253 prophase in *spo11* mutants owing to the role of RPA in pre-meiotic DNA replication, but then disappear 4
254 hours after induction of meiosis [74]. We found that at 4 hours, the majority of nuclei lacking RPA foci
255 contained Dmc1 foci in *spo11 dmc1-E157D* and *spo11 dmc1-E157D mei5* (100% and 96% of nuclei
256 lacking RPA had Dmc1 foci, respectively) (Figure 1e). We conclude that Dmc1-E157D forms DSB-
257 independent foci, suggesting that a substantial fraction of the foci observed in *SPO11⁺ dmc1-E157D* cells
258 represent off-pathway structures formed by binding unbroken chromosomal loci.

259 ***dmc1-E157D* bypasses Mei5, but not Rad51, with respect to meiotic CO formation**

260 To examine whether Dmc1-E157D is competent to carry out recombination in the absence of
261 Mei5, we performed 1D gel electrophoresis, followed by Southern blotting, to detect DNA double strand
262 breaks and formation of CO recombination products at the well-characterized recombination hotspot
263 *HIS4::LEU2* [75]. 1D gel electrophoresis at *HIS4::LEU2* can be used to detect DSB intermediates and IH
264 CO products. In addition, the same gels detect products that result from ectopic recombination between

265 the *HIS4::LEU2* locus and the native *LEU2* locus, which are separated by ~23 kilobases on chromosome
266 III [9,76]. As shown previously, DSBs accumulate and CO formation is very limited in *DMC1⁺ mei5*
267 (Figures 2a,b) [52,53]. In contrast, although *dmc1-E157D mei5* cells accumulate DSBs, these
268 intermediates are resolved by 24 hours, at which point CO formation is equivalent to wild-type (Figures
269 2a,b). In addition, whereas only 8.7% of *DMC1⁺ mei5* cells progress through a meiotic division, 50.0% of
270 *dmc1-E157D mei5* cells progress, a level nearly equivalent to *dmc1-E157D* (58.4%) (Figure 2b). This
271 shows that Dmc1-E157D bypasses the normal requirement for Mei5 during meiotic recombination.
272 Interestingly, ectopic recombination is elevated ~3.5-fold in *dmc1-E157D* and *dmc1-E157D mei5* relative
273 to wild-type.

274 Because Dmc1-E157D also bypasses Rad51 with respect to forming brightly staining foci, we
275 wanted to ask whether it similarly bypasses Rad51 for CO formation and DSB resolution at *HIS4::LEU2*.
276 Previous studies of *rad51* mutants showed that DSBs accumulate and undergo more extensive resection
277 than wild-type [70]. In addition, the final level of COs that form in *rad51* was reported to be 5-fold lower
278 than wild-type, and ectopic recombination is ~1.6-fold higher at 10 hours in sporulation medium [70,77].
279 We confirmed these phenotypes for the *rad51* single mutant (Figures 2a,b). Consistent with the failure of
280 *dmc1-E157D* to rescue the low spore viability phenotype of *rad51*, we found that *dmc1-E157D rad51*
281 accumulates hyper-resected DSBs (Figure 2a). Surprisingly, *dmc1-E157D rad51* makes fewer COs than
282 *rad51*, implying that the *dmc1-E157D rad51* double mutant is more defective than either the *dmc1-E157D*
283 single mutant or the *rad51* single mutant. Meiotic progression data similarly indicates that *dmc1-E157D* is
284 more defective than both *dmc1-E157D* and *rad51*; only 24.8% of *dmc1-E157D rad51* cells execute at
285 least one meiotic division, compared to 58.4% and 54.5% of *dmc1-E157D* cells and *rad51* cells
286 respectively (Figure 2b). Additionally, very little ectopic recombination is detected in *dmc1-E157D rad51*,
287 possibly reflecting the fact that there is less recombination overall, or a change in the pattern of formation
288 of joint molecules (JMs) or how they are resolved. Overall our results indicate that *dmc1-E157D* does not
289 bypass *rad51* with respect to resolution of meiotic DSBs.

290 The *dmc1-E157D mei5 rad51* triple mutant was similar to the *dmc1-E157D rad51* double, with the
291 triple displaying slightly more pronounced defects final CO levels (Figure 2a,b). We also found that the
292 efficiency of the first meiotic division is somewhat reduced in the *dmc1-E157D mei5 rad51* mutant

293 (11.3%) compared to the *dmc1-E157D rad51* (24.8%) mutant (Figure 2b). These results indicate that
294 recombination in *dmc1-E157D* displays a strong dependence on Rad51, but no dependence on Mei5,
295 unless Rad51 is absent.

296 Introduction of the *spo11* mutation into the *dmc1-E157D* and *dmc1-E157D mei5* backgrounds
297 rescued the meiotic progression defects observed for *dmc1-E157D* and *dmc1-E157D mei5*
298 (Supplemental Figure 2). Thus the meiotic progression defects observed in the *dmc1-E157D* background
299 are DSB-dependent. This finding suggests that although there are numerous DSB-independent Dmc1 foci
300 in these strains, these Dmc1-dsDNA complexes do not dramatically interfere with chromosome
301 segregation.

302 **Dmc1-mediated meiotic recombination is independent of Mei5-Sae3 in *dmc1-E157D***

303 We next sought to further characterize Dmc1-E157D-mediated recombination in the absence of
304 Mei5 by 2D gel electrophoresis and Southern blotting. Using this method, an array of JM recombination
305 intermediates can be detected at the *HIS4::LEU2* locus, including single-end invasions (SEIs), IS-double
306 Holliday junctions (IS-dHJs), IH-double Holliday junctions (IH-dHJs), and multi-chromatid joint molecules
307 (mcJMs) [78]. Representative 2D gel images are shown for each strain in Figure 3a. As expected, JM
308 formation is severely compromised in *mei5* (Figures 3a,b). In contrast, in *dmc1-E157D mei5*, JM
309 formation is efficient, with IH-dHJ levels equivalent to those in wild-type. IS-dHJs, however, are increased
310 ~3-fold, reducing the IH-dHJ/IS-dHJ ratio from 5.0 in wild-type to ~1.5 in *dmc1-E157D* (Figure 3b). *dmc1-*
311 *E157D mei5* phenocopies *dmc1-E157D*, which also has increased IS-dHJs and a reduced IH/IS ratio of
312 ~1.6. SEIs are observed at the same levels in *dmc1-E157D* and *dmc1-E157D mei5* mutants as in wild-
313 type (Figure 3b). Like IS-dHJs, mcJMs are increased relative to wild-type in both *dmc1-E157D* and *dmc1-*
314 *E157D mei5* (3.0-fold and 2.7-fold respectively). The similar array of JMs observed in *dmc1-E157D* and
315 *dmc1-E157D mei5* cells further indicates that Dmc1-E157D-mediated recombination occurs
316 independently of Mei5-Sae3. Although a decrease in the IH/IS ratio can be interpreted as a defect in the
317 mechanism of IH bias, this case is unusual in that the decreased ratio results from increased IS-dHJs,
318 with no reciprocal decrease in IH-dHJs. The fact that the level of IH-dHJs in *dmc1-E157D mei5* cells is
319 equivalent to that in wild-type suggests that the mechanism of homolog bias is intact in this mutant, and
320 reveals that Mei5-Sae3 is not required for IH bias. The data also suggest that the *dmc1-E157D* mutant is

321 a hyper-recombinant mutant, displaying higher than normal levels of IS-dHJs and mcJMs, as well as
322 increased ectopic COs.

323 ***dmc1-E157D rad51* exhibits a profound IH bias defect and a reduction in JM formation**

324 We next examined Dmc1-E157D-mediated recombination in the absence of Rad51 using 2D gel
325 electrophoresis. In a *rad51* mutant, Dmc1 carries out recombination, but there is a profound IH bias
326 defect, and most recombination occurs between sisters [69]. The IH-dHJ/IS-dHJ ratio in *rad51* is 0.4 and
327 the same ratio is displayed by *dmc1-E157D rad51* (Figures 4a,b). The defect in the IH/IS ratio is the result
328 of increased IS-dHJs and decreased in IH-dHJs. The profound defect in IH bias in *dmc1-E157D rad51*
329 contrasts with the *dmc1-E157D* single mutant, in which the IH-dHJ/IS-dHJ ratio is ~1.6. We conclude that
330 *rad51* is epistatic to *dmc1-E157D* with respect to its impact on partner choice. The impact of a *rad51*
331 mutation on the IH/IS ratio in *dmc1-E157D* cells further supports the view that the mechanism of homolog
332 bias is intact in *dmc1-E157D mei5* cells and therefore the conclusion that Mei5-Sae3 is not required for
333 homolog bias. The levels of IS-dHJs, IH-dHJs, SEIs, and mcJMs are all reduced roughly 2-fold in *dmc1-*
334 *E157D rad51* relative to *rad51* (Figure 4b); thus, the hyper-recombinant phenotype of *dmc1-E157D* cells
335 is Rad51-dependent. These findings are also consistent with the observation that CO levels in *dmc1-*
336 *E157D* are reduced about 2-fold by the *rad51* mutation (see Figure 2b).

337 **JM formation is absent in triple mutant *dmc1-E157D mei5 rad51***

338 We also analyzed the *dmc1-E157D mei5 rad51* triple mutant by 2D gel electrophoresis.
339 Surprisingly, while both *dmc1-E157D mei5* and *dmc1-E157D rad51* formed readily detectably levels of
340 JMs (Figures 3a,c), and Dmc1 foci were detected in *dmc1-E157D mei5 rad51* spread meiotic nuclei
341 (Figure 1c,d), no JMs were detected in the triple mutant (Figure 3c,d). Because *rad51* strains are
342 genetically unstable, we constructed an independent *dmc1-E157D mei5 rad51* diploid and repeated this
343 experiment to ensure that our original strain had not picked up an additional mutation that suppressed the
344 formation of JMs. Meiotic JMs were also undetectable in the duplicate *dmc1-E157D mei5 rad51* strain
345 (Supplemental Figures 3a,b). These 2D gel analyses are consistent with our findings that only ~10% of
346 cells progress through a meiotic division in *dmc1-E157D mei5 rad51*, and that there is hyper-resection
347 and limited CO formation in this strain (Figures 2a,b). We conclude that recombination is further
348 compromised in the triple mutant *dmc1-E157D mei5 rad51* than in either of the double mutants. These

349 results provide additional evidence that although Dmc1-E157D's activity is essentially Mei5-Sae3
350 independent in *RAD51*⁺ cells, Mei5-Sae3 can promote limited Dmc1-E157D activity when Rad51 is
351 absent.

352 **The defects associated with *dmc1-E157D* and *dmc1-E157D mei5* are independent of Rad51's**
353 **catalytic activity**

354 One possible explanation for the results we obtained from our JM analysis is that the *dmc1-*
355 *E157D* mutation changes the behavior of Dmc1 in a manner that activates the strand exchange activity of
356 Rad51. This possibility is emphasized by previous results suggesting that Dmc1 itself inhibits Rad51's
357 strand exchange activity [79,80]. Normally, Rad51's strand exchange activity is repressed by Dmc1 and
358 by the meiosis-specific Rad51 inhibitor Hed1 [3,66]. However, it was important to determine if Rad51's
359 strand exchange activity plays a greater role in promoting recombination in *dmc1-E157D* cells than in
360 wild-type [80]. To test this, we crossed the *rad51-II3A* mutation into our *dmc1-E157D* strains. The three
361 alanine substitutions coded by *rad51-II3A* eliminate DNA binding site II, the secondary, low affinity DNA
362 binding site required for homology searching. Rad51-II3A forms filaments, but lacks the ability to catalyze
363 D-loop formation [3]. The results indicate that the *rad51-II3A* mutation does not alter the efficiency of JM
364 formation in the *dmc1-E157D* mutant (Supplemental Figures 4a,b). This observation indicates that Dmc1,
365 not Rad51, promotes the majority of homology search and strand exchange in *dmc1-E157D* cells, as is
366 the case in wild-type cells. Thus, the hyper-recombinant phenotype observed in *dmc1-E157D* results from
367 increased Dmc1 activity rather than activation of Rad51's activity. On the other hand, *rad51-II3A* causes a
368 greater reduction in spore viability in a *dmc1-E157D* background than in a wild-type background (Table 1,
369 17.0% and 82.9%, respectively, $p < 0.01$). The modest reduction in viability seen in *rad51-II3A* single
370 mutants was previously interpreted to suggest that Rad51's strand exchange is only required at a small
371 subset of the roughly 200 DSB sites where Dmc1-dependent DSB repair fails [3]. In the context of this
372 interpretation, the data presented here can be explained if the fraction of attempted recombination events
373 that require Rad51's strand exchange activity, although still small, is higher in *dmc1-E157D* than that in
374 wild-type.

375 **Meiotic two-hybrid analysis indicates that direct Rad51-Dmc1 interaction is independent of Mei5**

376 The results presented in Figure 3 show that Rad51 can impact Dmc1's activity in the absence of
377 Mei5-Sae3. To determine if Rad51's influence on Dmc1 can be explained by direct interaction of the two
378 proteins, we carried out meiotic two-hybrid analysis. A previous two-hybrid study in budding yeast using
379 the conventional mitotic method detected a low level of direct interaction between Rad51 and Dmc1,
380 although the authors of that study did not ascribe significance to the interaction because it was much
381 weaker than that observed for homotypic Rad51-Rad51 and Dmc1-Dmc1 interactions [81]. We wished to
382 determine if Mei5-Sae3 enhanced the interaction between the two proteins and therefore used the meiotic
383 two-hybrid method to test the interaction in a cell type that expresses the accessory protein. As in the
384 previous study, the level of interaction observed for Rad51-Dmc1 was much lower than that in the Rad51-
385 Rad51 and Dmc1-Dmc1 homotypic controls, but nonetheless reproducibly higher than the background
386 level observed in empty vector controls (Supplemental Figure 5). Importantly an equivalent two-hybrid
387 signal was detected in a *mei5* null background as in a wild-type background indicating that, in this system,
388 Rad51-Dmc1 interaction is independent of Mei5-Sae3.

389 **Super-resolution imaging of *dmc1-E157D* mutants reveals abnormalities in Dmc1 and RPA foci**

390 Because Dmc1-E157D forms foci at high density, we expected that the wide-field microscopy
391 method was not resolving closely spaced foci. Therefore, in order to obtain more accurate focus
392 measurements, we re-examined chromosome spreads using STED microscopy, which improves the
393 resolution limit from around 200 nanometers (nm) to under 50 nm (see Methods Section, Supplemental
394 Figure 6a). For each strain, we imaged at least 13 randomly selected RPA-positive nuclei. The average
395 number of RPA foci detected was lowest in wild-type (70.0 ± 22.2 foci). All other strains displayed higher
396 average focus counts including *rad51* (140.5 ± 44.9 foci), *dmc1-E157D* (111.5 ± 28.8 foci), *dmc1-E157D*
397 *mei5* (130.8 ± 21.2 foci), *dmc1-E157D rad51* (132.0 ± 21.7 foci), and *dmc1-E157D mei5 rad51* ($131.3 \pm$
398 38.6 foci) (Figure 4b). We also measured focus lengths (Figure 4c), and found that wild-type RPA foci are
399 the shortest (76.8 ± 27.0 nm), while *rad51*, *dmc1-E157D rad51*, and *dmc1-E157D mei5 rad51* foci are all
400 significantly longer (134.0 ± 70.4 nm, 136.0 ± 77.8 nm, 130.8 ± 63.8 nm respectively; $p < 0.01$, Wilcoxon
401 test), but not significantly different from one another (pairwise $p = 0.53, 0.60, \text{ and } 0.94$, respectively). The
402 fact that RPA foci are longer in these strains is unsurprising given that we observed hyper-resection in all
403 of these strains by one-dimensional gel electrophoresis (Figure 2a). *dmc1-E157D* and *dmc1-E157D mei5*

404 mutant RPA foci are significantly different from both wild-type and *rad51* mutants (107.4 ± 49.5 nm, $97.7 \pm$
405 39.6 nm respectively; $p < 0.01$), being an intermediate average length between the two.

406 The average number of Dmc1 foci per nucleus was similar in wild-type and *rad51* single mutants
407 (26.9 ± 17.7 foci and 23.3 ± 12.8 foci, respectively, Figure 4b). All *dmc1-E157D* strains displayed higher
408 than normal focus counts including *dmc1-E157D* (114.0 ± 21.0 foci), *dmc1-E157D mei5* (119.2 ± 25.6
409 foci), *dmc1-E157D rad51* (105.3 ± 27.0 foci), and *dmc1-E157D mei5 rad51* (106.8 ± 23.8 foci) (Figure
410 4b). This result is expected given that Dmc1-E157D forms numerous brightly staining foci in the absence
411 of DSBs, whereas wild-type Dmc1 does not (Figure 1e). We also measured the lengths of these Dmc1
412 foci, and found that Dmc1 foci are significantly shorter in *rad51* (82.5 ± 30.0 nm, $p < 0.01$, Wilcoxon test)
413 than wild-type (97.1 ± 38.8 nm) (Figure 4c), consistent with previous wide-field microscopy analyses [68].
414 Dmc1 foci are longer in all *dmc1-E157D* strains, including *dmc1-E157D* (134.1 ± 61.5 nm, $p < 0.01$),
415 *dmc1-E157D mei5* (147.1 ± 66.4 nm, $p < 0.01$), *dmc1-E157D rad51* (161.9 ± 78.9 , $p < 0.01$), and *dmc1-*
416 *E157D mei5 rad51* (143.3 ± 64.7 nm, $p < 0.01$) relative to wild-type (Figure 4c).

417 Although measurements of Dmc1 focus lengths shows that Dmc1-E157D makes longer than
418 normal filaments overall, the fact that the protein likely forms high levels of off-pathway foci in addition to
419 forming foci at sites of recombination raises the possibility that the long filaments observed might only be
420 off-pathway forms, with no appreciable change in the average length of recombinogenic filaments.
421 Furthermore, the fraction of recombinogenic foci could differ in different strains. For example, off-pathway
422 Dmc1 foci a larger fraction of the total in *dmc1-E157D* strains than in wild-type and *rad51*. To provide
423 evidence that recombinogenic foci are longer on average, we examined the lengths of Dmc1 foci that
424 colocalized with RPA. Given that all of the mutants have more RPA foci and some have more Dmc1 foci
425 (Figure 4b), the level of fortuitous colocalization is expected to be higher in the mutants than in wild-type.
426 We therefore estimated the frequency of fortuitous colocalization in all strains by a previously described
427 method [74]. This method may yield an overestimate because the most focus dense region of each
428 nucleus was used in the analysis. We eliminated any nuclei from our analysis if the level colocalization
429 observed in the experimental image did not exceed the estimated frequency of fortuitous colocalization by
430 more than 5%. Because both RPA and Dmc1 foci are more numerous in *dmc1-E157D rad51* and *dmc1-*
431 *E157D mei5 rad51* (Figure 4b), and because both RPA and Dmc1 foci are on average larger in these

432 strains (Figure 4c), the density of foci is much higher, and we were unable to identify a subset of Dmc1
433 foci in these strains that unambiguously colocalize with RPA (90.2% experimental and 91.4% fortuitous
434 colocalization in *dmc1-E157D rad51*; 81.1% true and 80.0% fortuitous colocalization in *dmc1-E157D mei5*
435 *rad51*). In contrast, 10/13 nuclei wild-type nuclei (35.5% experimental and 18.8% fortuitous), 10/13 *dmc1-*
436 *E157D* nuclei (70.1% experimental and 58.6% fortuitous colocalization), and 6/13 *dmc1-E157D mei5*
437 nuclei (69.1% experimental and 57.1% fortuitous colocalization) met our criteria for analysis, indicating
438 that the RPA-colocalization provides a meaningful criterion to identify a subset of Dmc1 foci enriched for
439 recombinogenic as opposed to off-pathway structures. The average contour length of Dmc1 filaments
440 that colocalized with RPA was 118.9 ± 40.0 nm in wild-type, or ~ 100 nucleotides, similar to the
441 corresponding value obtained using dSTORM, a different super-resolution light microscopy method [26].
442 The average focus length for RPA colocalizing Dmc1 foci in *dmc1-E157D* was significantly longer than in
443 wild-type (149.5 ± 66.8 nm, or ~ 160 nucleotides, Figure 4d, $p < 0.01$, Wilcoxon test), and different from the
444 total Dmc1 foci lengths in *dmc1-E157D* cells (134.1 ± 61.5 nm, Figure 4c). The average focus length for
445 RPA colocalizing Dmc1 foci in *dmc1-E157D mei5* was also significantly longer than in wild-type ($168.0 \pm$
446 66.4 nm, or ~ 190 nucleotides, $p < 0.01$), and different from the total Dmc1 foci lengths in that background
447 (147.1 ± 66.4 nm, Figure 4c). This finding indicates that not only does Dmc1-E157D make longer foci
448 overall, in *dmc1-E157D* and *dmc1-E157D mei5*, where we observe the hyper-recombinant phenotype,
449 Dmc1 filaments associated with RPA are significantly longer than wild-type.

450 **Rhd54 promotes meiotic progression in *dmc1-E157D* cells**

451 The cytological results presented above suggest that Dmc1-E157D is more likely than Dmc1-WT
452 to form off-pathway filaments on dsDNA. DSB-independent foci are only easily detected for Dmc1-WT
453 when Rhd54, the key translocase involved in disassembling them, is absent [41]. This observation
454 suggested that Dmc1-E157D might be more resistant to dsDNA dissociation by Rhd54. To determine
455 whether Rhd54 was active in *dmc1-E157D* mutants, we constructed the *dmc1-E157D rdh54* double
456 mutant. If Rhd54 is inefficient at promoting Dmc1-E157D dissociation from dsDNA, loss of Rhd54 in the
457 *dmc1-E157D* background should be inconsequential. Instead, we find that although both *dmc1-E157D*
458 and *rdh54* single mutants progress through meiosis to form tetrads in which roughly 50% of spores are

459 viable, the *dmc1-E157D rdh54* double mutant arrested in prophase and failed to form spores (Table 1;
460 Supplemental Figure 7). Thus, Rdh54 is active in *dmc1-E157D* cells.

461 **Mei5-Sae3 is not required for the DSB-independent foci formed by Dmc1-WT protein in the**
462 **absence of Rdh54**

463 Dmc1-E157D differs from Dmc1-WT in that it forms high levels of off-pathway foci and does so
464 independently of Mei5-Sae3. This suggests that although the mutant bypasses the requirement for Mei5-
465 Sae3 with respect for forming recombinogenic foci, it might not fully recapitulate Mei5-Sae3 function
466 because Mei5-Sae3's has only been shown to display DSB-dependent foci; it was not known if Mei5-
467 Sae3 is also required for the off-pathway Dmc1 complexes that accumulate when disassembly of dsDNA
468 bound structures is blocked by an *rdh54* mutation. Therefore, to determine if Mei5-Sae3 is normally
469 required for Dmc1 to form nascent complexes on dsDNA *in vivo*, we compared Dmc1 focus formation in
470 *spo11 rdh54 mei5* to that in the *spo11 rdh54* double mutant; a *spo11* single mutant served as negative
471 control. The controls generated the expected results with *spo11 rdh54* nuclei displaying an average of
472 37 ± 14 Dmc1 foci/nucleus and *spo11* nuclei an average of only 3 ± 4 foci/nucleus (Supplemental Figure 8).
473 The *spo11 rdh54 mei5* triple mutant displayed an average of 37 ± 13 foci, like the positive control,
474 indicating that focus formation in *spo11 rdh54* is Mei5 independent. Thus, a key component of Mei5-Sae3
475 function appears to be specific to promoting filaments on ssDNA. Dmc1-E157D appears to bypass the
476 requirement for Mei5-Sae3 for filament formation on ssDNA, but does so without displaying the ssDNA-
477 specific function normally provided by Mei5-Sae3.

478

479 **Discussion**

480 **The mechanism of Mei5-Sae3-mediated Dmc1 filament formation**

481 Dmc1-E157D was designed to mimic RecA-E96D. The RecA-E96D mutation shortens the length
482 of a critical amino acid side chain in the ATPase active site, increasing the distance between the water
483 molecule that acts as the nucleophile for hydrolysis, and the activating carboxylate [71]. The mutation
484 dramatically reduces that rate of ATP hydrolysis thereby maintaining RecA in the ATP-bound form, which
485 is active for DNA binding, homology search, and strand exchange. Due to the high sequence
486 conservation of this site, Dmc1-E157D is very likely to be defective in ATPase activity, like RecA-E96D.

487 Assuming this prediction is correct, our results provide *in vivo* support for the conclusion of Chi and
488 colleagues that Swi5-Sfr1 acts to stabilize Rad51 filaments by promoting ADP release, thereby
489 maintaining the filament in the active, ATP-bound form [59]; a mutation designed to favor the ATP bound
490 form of Dmc1 bypasses the normal requirement for Mei5-Sae3. On the other hand, the regulatory defects
491 observed in Dmc1-E157D suggest that the function of Mei5-Sae3-mediated regulation involves more than
492 overall enhancement of Dmc1 filament stability, because the Dmc1-E157D mutant displays abnormally
493 high levels of *spo11*-independent Dmc1-E157D binding to chromosomes (Figure 1e). This finding
494 suggests that stabilizing the ATP-bound form of Dmc1 alone is insufficient to account for the mechanism
495 of Mei5-Sae3 function. Supporting this view, we find that although Mei5-Sae3 is required for cytologically
496 detectable Dmc1 focus formation at sites of DSBs in wild-type cells, it is not required to observe the off-
497 pathway dsDNA-bound foci formed on dsDNA by Dmc1-WT in *Rdh54* deficient cells (Supplemental
498 Figure 8). This interpretation is consistent with prior observation of direct binding of Mei5-Sae3 to the
499 ssDNA-specific binding protein RPA as well as the ability of Mei5-Sae3 to enhance Dmc1 activity in the
500 presence of RPA [50,57,60]. Thus, Mei5-Sae3 appears to combine the ability to enhance Dmc1 filament
501 stability with the ability to specifically promote filament formation on ssDNA rather than dsDNA.

502 The ability of Dmc1-E157D to form functional filaments on ssDNA *in vivo* in the absence of Mei5-
503 Sae3, and to do so by a mechanism involving filament stabilization, opens the possibility that
504 recruitment/nucleation of Dmc1 filaments on RPA coated ssDNA in normal cells is independent of Mei5-
505 Sae3. Given that Mei5-Sae3 binds directly to both Dmc1 and RPA [52,53,60], we continue to favor
506 models in which Mei5-Sae3 plays a role in recruitment/nucleation of Dmc1 filaments. We note, however,
507 that Dmc1 could be recruited to sites of DSBs through its interactions with RPA [50], and that nucleation,
508 but not filament elongation, could be Mei5-Sae3 independent. Dmc1 nucleation events might be
509 undetected in the absence of Mei5-Sae3 because the resulting filaments never elongate to lengths
510 sufficient to reach the threshold of cytological detection. It is also possible that Rad51 is normally partially
511 responsible for Dmc1 recruitment/nucleation, in addition to its roles in filament stabilization and homolog
512 bias. These considerations highlight the need for further studies on the mechanism of Dmc1
513 recruitment/nucleation on RPA coated ssDNA tracts *in vivo*.

514 **The role of Rad51 in Dmc1 filament dynamics**

515 The absence of foci observed in *mei5*, *sae3*, and *mei5 sae3* mutants, and the dimmer foci
516 observed in *rad51* mutants, indicates that normal Dmc1 nucleoprotein filament formation involves both
517 proteins. The fact that recombination and DSB-dependent focus formation in *rad51* yeast depends on
518 Mei5-Sae3 suggests that Mei5-Sae3 is epistatic to Rad51. Furthermore, formation of brightly staining
519 Mei5-Sae3 foci depends on Rad51, as does formation of brightly staining Dmc1 foci [52,68]. These
520 dependency relationships raised the possibility that Rad51's ability to influence Dmc1 filaments might
521 require a direct interaction between Rad51 and Mei5-Sae3 [82]. However, the data presented here
522 indicate that Rad51 promotes formation of functional Dmc1 filaments on ssDNA independently of Mei5-
523 Sae3, thus Rad51's normal influence on Dmc1 filament dynamics does not require, and may not involve,
524 Mei5-Sae3 binding to Rad51.

525 Our data clearly demonstrate that *dmc1-E157D* functions independent of Mei5-Sae3, yet the
526 mutant is more dependent on Rad51 than the wild-type protein. Whereas *dmc1-E157D mei5* forms COs
527 at a level nearly equivalent to wild-type, *dmc1-E157D rad51* suffers a dramatic reduction in CO formation,
528 and experiences hyper-resection (Figures 2b,4c). In addition, 2D gel electrophoresis shows that JM
529 formation in *dmc1-E157D mei5* is equivalent to *dmc1-E157D*, while the JMs formed in the *dmc1-E157D*
530 *rad51* background are significantly reduced relative to *dmc1-E157D*, and show an IH bias defect like the
531 *rad51* single mutant (Figures 3b, 3d). Thus, a mutation that alleviates the need for one accessory factor,
532 Mei5-Sae3, makes Dmc1 more dependent on a second accessory factor, Rad51. This finding provides
533 further evidence that Mei5-Sae3 and Rad51 functions are not interdependent with respect to enhancing
534 the formation of functional Dmc1 filaments. If this were the case, a mutation that bypasses the
535 requirement for one factor would also bypass the requirement for the second factor. This model accounts
536 for the partial dependency of Mei5-Sae3 foci on Rad51; the reduction of Mei5-Sae3 focus intensity
537 observed in *rad51* mutants is expected if Dmc1 filaments are bound along their lengths by Mei5-Sae3,
538 and loss of Rad51 results in shorter Dmc1 filaments.

539 Rad51 is likely to impact Dmc1 filament dynamics by direct interaction. Although a previous study
540 did not ascribe significance to the low level of interaction detected between budding yeast Rad51 and
541 Dmc1 [81], two-hybrid studies in other organisms detected significant levels of Rad51-Dmc1 interaction,
542 albeit at low levels compared to homotypic interactions [83-85]. Budding yeast Rad51 binds Dmc1 directly

543 when pure proteins are mixed [50], consistent with similar observations in other organisms [83-85]. Using
544 the meiotic two-hybrid method, we were able to detect Rad51-Dmc1 interaction during meiotic prophase
545 of budding yeast, and to show that this interaction does not depend on Mei5-Sae3. These findings
546 provide additional evidence that Rad51 and Mei5-Sae3 influence Dmc1 DNA binding dynamics
547 independently. The finding that Rad51-Dmc1 interaction occurs, but is weaker than homotypic
548 interactions, is consistent with a single molecule study that showed mixtures of Rad51 and Dmc1 form
549 predominantly homo-filaments on DNA [21], and with prior cytological studies that showed the foci formed
550 by Rad51 and Dmc1 lie adjacent to one another rather than being perfectly colocalized [51,81,86]. Finally,
551 we note that direct interaction between the two proteins can account for the observation that Rad51 can
552 stimulate Dmc1-mediated D-loop formation in the absence of other proteins [3].

553 How might Mei5-Sae3 and Rad51 promote filament stability by independent mechanisms? There
554 are at least two basic mechanisms that could contribute to filament stability. First, an accessory protein
555 could promote the high-affinity ssDNA binding form. Second, if a strand exchange protein is normally
556 subject to enzymatically-driven disassembly, an accessory protein might act by specifically blocking the
557 activity of that enzyme. Mei5-Sae3's role in filament stabilization *in vivo* almost certainly involves direct
558 enhancement of DNA binding activity during nucleation and/or elongation, as is the case for Mei5-Sae3
559 homolog Sfr1-Swi5 [62]. Rad51 might also enhance binding directly, by reducing the off-rate of protomers
560 from filaments. For example, a Rad51 monomer bound to the end of a Dmc1 filament might drastically
561 reduce the off-rate of the adjacent Dmc1 protomer with a strong overall effect on filament stability, given
562 that disassembly of filaments is expected to occur from filament ends [87].

563 Alternatively, Rad51 may block a mechanism that actively dissociates Dmc1 filaments. Although
564 no active assembly mechanism has been identified for Dmc1 filaments, active disassembly could involve
565 a helicase mechanism, similar to that mediated by UvrD and Srs2 [16-19]. One observation that appears
566 to be at odds with the idea that Rad51 functions by blocking an Srs2-like mechanism is that Rad51 can
567 stimulate Dmc1's D-loop activity in a purified system that does not include an ssDNA-specific helicase.
568 However, it is possible that the *in vitro* activity of Rad51 in stimulating Dmc1 does not fully recapitulate the
569 *in vivo* function of the protein. This possibility is emphasized by previous work on the Rad51 accessory
570 protein Rad55-Rad57. Both subunits of the Rad55-Rad57 heterodimer are structurally similar to Rad51.

571 Rad55-Rad57 stimulates Rad51 activity *in vitro*, but *in vivo* it functions to limit the Rad51 strippase activity
572 of Srs2 [88,89]. Thus, Rad51's impact on Dmc1 activity *in vitro* might similarly not fully represent its *in vivo*
573 role in promoting stable Dmc1 filaments.

574 A model invoking inhibition of Dmc1-ssDNA filament disassembly can account for the fact that
575 *dmc1-E157D rad51* forms fewer JMs relative to *DMC1⁺ rad51* (Figure 3d). Like Dmc1-E157D, the Rad51
576 ATPase mutant Rad51-K191R is defective in recruitment to DSB-associated tracts of ssDNA *in vivo*. The
577 DNA binding defect of Rad51-K191R is partially suppressed by deletion of *SRS2* or by overexpression of
578 *RAD54* [45,46]. These findings suggest that the recruitment defect displayed by Rad51-K191R results
579 from a combination of the protein's DNA binding defect, increased off-pathway dsDNA binding, and active
580 disassembly of the Rad51-K191R filaments that do form at DSB-associated tracts of ssDNA [47].

581 If Dmc1-E157D filaments form more slowly than wild-type filaments as a result of increased off-
582 pathway binding and thus a decreased pool of free Dmc1 protomers, Dmc1-E157D filaments may be
583 acutely sensitive to disassembly and/or end dissociation, thus both models can explain Dmc1-E157D's
584 increased dependency on Rad51. In addition, these models can account for the more severe phenotype
585 of the *dmc1-E157D mei5 rad51* triple mutant compared to the *dmc1-E157D rad51* double mutant as a
586 consequence of Mei5-Sae3 having a limited ability to block dissociation, or being able to promote fast
587 reassembly. Such an activity of Mei5-Sae3 might be inconsequential for Dmc1-E157D-DNA binding
588 dynamics *in vivo* when Rad51 is present, explaining why the phenotypes of *dmc1-E157D* and *dmc1-*
589 *E157D mei5* are nearly identical.

590 **Mei5-Sae3 is not required for IH bias**

591 The results presented here also reveal for the first time that although both Rad51 and Mei5-Sae3
592 promote the formation of stable Dmc1 filaments, Mei5-Sae3 differs from Rad51 in that Mei5-Sae3 is not
593 required for homolog bias while Rad51's function is. This conclusion could not have been arrived at
594 based on earlier observations because recombination is blocked prior to formation of joint molecules in
595 *mei5 DMC1⁺* and *sae3 DMC1⁺* cells; bypass of the requirement for Mei5-Sae3 for formation of functional
596 filaments allowed us to assess the role of Mei5-Sae3 during choice of recombination partner at the D-loop
597 formation stage. Previous work showed that Rad51 and Dmc1 are both required for homolog bias
598 [69,80]. The results here show that the cooperation between Rad51 and Dmc1 required for IH bias

599 involves a Rad51-dependent mechanism that is independent of Mei5-Sae3. This interpretation is
600 consistent with the fact that, in other species, homologs of Mei5-Sae3 regulate Rad51 activity, suggesting
601 that the Mei5-Sae3 family of accessory proteins solves a problem common to both Rad51 and Dmc1, and
602 not unique to meiotic recombination.

603 Chromatin immunoprecipitation experiments have shown that cells lacking both Rdh54 and
604 Rad54 fail to recruit Dmc1 to DSB hotspots as a consequence of sequestration caused by off pathway
605 DNA binding. The failure to recruit Dmc1 to tracts of ssDNA accounts for the hyper-resection seen in
606 *rad54 rdh54* double mutants [41,90]. Given that Dmc1-E157D forms foci in the absence of DSBs, and that
607 it is modeled on RecA-E96D, which displays a lower than normal off-rate for dsDNA binding, one might
608 expect that Dmc1-E157D is less efficiently removed from dsDNA by Rdh54 (and Rad54). Surprisingly, we
609 find no evidence for a decrease in CO formation or for hyper-resection in *dmc1-E157D* (Figures 2a,b).
610 Moreover, there is no accumulation of SEIs, which might be expected if Rdh54 were unable to remove
611 Dmc1 from the 3' end of the heteroduplex DNA to allow for recombination-associated DNA synthesis
612 (Figures 3a,b). We also find that the high spore viability and meiotic progression observed in *dmc1-*
613 *E157D* mutants is strongly dependent of Rdh54, indicating that Rdh54 is active in *dmc1-E157D* mutants
614 (Table 1, Supplemental Figure 4). Thus, although Dmc1-E157D forms more off-pathway filaments than
615 Dmc1-WT, Rdh54 appears to be capable of dissociating them.

616 **Dmc1-E157D forms abnormally long filaments and is hyper-recombinant for certain recombination** 617 **events**

618 Although levels of IH CO intermediates and products are similar to those in wild-type, *dmc1-*
619 *E157D* and *dmc1-E157D mei5* display higher than normal levels of certain types of recombination
620 intermediates and products including IS-dHJs, mcJMs, and ectopic COs. For simplicity, we will refer to
621 these unusual types of recombination events collectively as “aberrant,” but we emphasize that all three
622 types are observed at low levels in wild-type. IS-dHJs, mcJMs, and ectopic COs are all elevated about 3-
623 fold in *dmc1-E157D* and *dmc1-E157D mei5* cells (Figures 2b,3b,3d). The combination of aberrant
624 recombination phenotypes observed in *dmc1-E157D* cells is reminiscent of that reported for *sgs1*, *top3*,
625 and *rmi1* mutants during meiosis [91-93]. Sgs1, Top3, and Rmi1 have been shown to form a complex,
626 STR, that disassembles D-loops [94-96]. In addition, during mitotic recombination, STR was shown to

627 have a role in disassembling aberrant invasion events in which a single Rad51 filament invades two or
628 more donor molecules (“multi-invasions”, or MIs) [97]. This role of STR in MI disassembly was proposed
629 to account for at least some of the phenotypes observed in the absence of Sgs1, Top3, or Rmi1 during
630 meiosis [93]. In this context, maturation of a MI into a mcJM, followed by resolution of the MI, can account
631 for the increase in mcJMs, IS-dHJs, and ectopic recombination observed in these mutants [98]. Further
632 evidence that MIs account for the meiotic STR mutant phenotypes is the fact that both MIs and JMs in the
633 *sgs1*, *top3*, or *rmi1* mutant backgrounds are highly dependent on structure-selective nucleases Mus81-
634 Mms4, Slx1-Slx4, and Yen1 [92,93,97,99-101].

635 Two possibilities account for why *dmc1-E157D* and *dmc1-E157D mei5* are phenotypically similar
636 to STR mutants. Dmc1-E157D may form the same number of aberrant intermediates as wild-type, but
637 STR-mediated disassembly could be rendered less efficient as a consequence of enhanced binding
638 activity of Dmc1-E157D compared to Dmc1-WT. Arguing against this possibility is the fact that there is no
639 increase in SEIs in *dmc1-E157D* and *dmc1-E157D mei5* cells compared to wild-type (Figures 3b, 3d),
640 which is expected if the mutant protein prevents nascent D-loop disruption. Moreover, we showed that
641 Rdh54 promotes meiotic progression in *dmc1-E157D* (Table 1, Supplemental Figure 7), implying that
642 Rdh54 is competent to remove Dmc1-E157D from dsDNA.

643 An alternative model to account for the defects associated with *dmc1-E157D* and *dmc1-E157D*
644 *mei5* is that Dmc1-E157D makes more aberrant D-loops than Dmc1-WT. In this model, STR, and possibly
645 other helicases, disassemble aberrant D-loops as normal, but the mutant protein generates more MIs
646 than Dmc1-WT. The two regions of homology engaged in such MI events could be on one sister and one
647 homolog, or on both of the homologs, likely engaging one template at the allelic site, and one at the
648 ectopic site. The formation of the MIs can account for the increased mcJMs, while processing of MIs to
649 yield fully repaired chromatids can explain the increases in IS-dHJs and ectopic COs [98]. Drawing on the
650 “intersegmental contact sampling” model of homology search [102], we propose Dmc1-E157D makes
651 more MIs as a consequence of making longer filaments (Figure 5). The intersegmental contact sampling
652 model maintains that a filament has a polyvalent interaction surface capable of simultaneously searching
653 multiple, non-contiguous DNA regions for homology [102]. Longer filaments are able to search duplex
654 DNA more efficiently, as a consequence of being able to engage in a greater number of simultaneous

655 interactions. We have demonstrated that Dmc1-E157D forms longer filaments *in vivo* (Figure 4c). We
656 posit that because filaments are longer, Dmc1-E157D engages in a higher number of simultaneous
657 searching interactions that results in more frequent homology-dependent engagement of two different
658 regions of homology by a single filament. In addition, though these aberrant recombination events are
659 increased in *dmc1-E157D*, they also make up a substantial fraction of the recombination events observed
660 in wild-type [91,97]. Consistent with this finding, 14% of wild-type Dmc1 foci that colocalized with RPA or
661 ~1.2 foci/nucleus were longer than 149 nanometers in length, the average length of Dmc1-E157D foci
662 that colocalize with RPA in *dmc1-E157D* (Figure 4d). This finding suggests that although most foci are
663 much shorter than 149 nanometers in wild-type, long filaments do occasionally form. Supporting the
664 proposal that longer than normal filaments are responsible for higher than normal levels of MIs, previous
665 work showed that (1) if longer ssDNA substrates are used, there is a higher incidence of MI formation
666 [103]; and (2) Rad55-Rad57 promotes both longer Rad51 filaments and the formation of MIs [89,98].

667 The aberrant event hyper-recombinant phenotype displayed by Dmc1-E157D is Rad51-
668 dependent. The mechanism responsible for Rad51's role in promoting the aberrant hyper-recombinant
669 activity of Dmc1-E157D remains to be determined. Analysis of RPA co-localized foci provided evidence
670 that Dmc1-E157D forms longer filaments on ssDNA in otherwise wild-type cells and in *mei5* single
671 mutants. The mutant protein also forms long filaments on dsDNA, given that long filaments are observed
672 in *spo11* mutants. Because both RPA and Dmc1 foci counts are increased in *dmc1-E157D rad51* and
673 *dmc1-E157D mei5 rad51* mutants (Figure 4b), and because both RPA and Dmc1 foci are also larger in
674 these mutants (Figure 4c), it was not possible to identify a sub-population that we could be confident was
675 enriched for ssDNA bound structures in these mutants. As a result, it is unclear if the dependency of
676 Dmc1-E157D's hyper-recombinant phenotype on Rad51 reflects a requirement for Rad51 in forming long
677 Dmc1 filaments on ssDNA, or if Rad51 plays some other role in promoting the high level of aberrant
678 recombination events observed in Dmc1-E157D. It is clear, however, that Rad51's homology search and
679 strand exchange activities are not required for the aberrant hyper-recombinant phenotype observed in
680 *dmc1-E157D* cells because the *rad51-II3A* mutation had no impact on the phenotype.

681 We speculate that the lengths of RecA-family strand exchange filaments are limited by regulatory
682 mechanisms that evolved to prevent homology-dependent translocations and other genome

683 rearrangements. Limiting filament lengths may limit the ability of filaments to simultaneously engage more
684 than one homologous target sequence. In this regard, it is relevant that the single molecule study that
685 provided evidence for intersegmental transfer did not detect any homology-dependent target engagement
686 with the shortest ssDNA substrate examined, which was 162 nucleotides in length [102]. However, *in*
687 *vivo*, Dmc1 filaments are typically ~100 nucleotides in wild-type cells (Figure 4c) [26]. Thus, it is possible
688 that the cost of MIs to genome stability has limited the length of strand exchange filaments such that
689 intersegmental searching is limited or prevented *in vivo*. Alternatively, homology search may proceed by
690 an intersegmental contact sampling mechanism, but filament lengths may nonetheless be limited to avoid
691 genome-destabilizing MIs.

692

693 **Materials and Methods**

694 **Yeast Strains**

695 The yeast strains used in this study are listed in Supplemental Table 1. All yeast strains are
696 isogenic derivatives of strain SK-1.

697 To construct the *dmc1* point mutants, DKB plasmid pNRB628 containing the *DMC1* open reading
698 frame, a 701 base pair upstream homology arm, the *TEF1* promoter, the *natMX4* open reading frame, the
699 *ADH1* terminator, and a 40 base pair downstream homology arm, was modified by Gibson assembly to
700 include the desired point mutations. *dmc1::LEU2-URA3-KAN* haploid yeast (DKB129, DKB130) were
701 transformed with a linear PCR fragment containing the homology arms, the mutated *dmc1* open reading
702 frame, and the *natMX4* (for resistance to nourseothricin sulfate, or cloNAT) selectable marker. Yeast were
703 outgrown in 5 milliliters liquid YPDA for 4.5 hours at 30°C in a culture rotator, then plated on selective
704 media and allowed to grow at 30°C for 3 days. After 3 days, colonies were struck out on the selective
705 media and on 5-fluoroorotic acid (5-FOA), which selects against *URA3*⁺ yeast and therefore identifies
706 clones that have lost the *dmc1::LEU2-URA3-KAN* allele. Those colonies that grew on the cloNAT media
707 and did not grow on the 5-FOA plates were tested to confirm proper targeting by polymerase chain
708 reaction, and then confirmed via sequencing.

709 **Meiotic Time Courses**

710 Yeast cultures were induced to undergo synchronous meiosis as described previously [51].

711 Appropriate samples were collected at time points indicated in figures.

712 **Spore viability**

713 Spore viability was determined by tetrad dissection as the percent of spores that germinate and
714 form a colony on a YPDA plate relative to the number expected if all dissected spores had lived.

715 **Preparation and staining of spread yeast nuclei**

716 Surface-spreading and immunostaining of meiotic yeast chromosomes on glass slides was
717 performed as described previously [104]. Primary antibodies were used at the following dilutions: purified
718 anti-goat Dmc1 bleed #4 DKB antibody #192 (1:800), anti-rabbit Rad51 bleed #2 DKB antibody #159
719 (1:1000), anti-rabbit RFA2 (1:1000), and anti-rabbit Hop2 bleed #3 DKB antibody #143 (1:1000).
720 Secondary antibodies were used at a dilution of 1:1000 and included: Alexa Fluor 488 chicken anti-goat
721 (Invitrogen by ThermoFisher Scientific), Alexa Fluor 594 donkey anti-rabbit (Invitrogen by ThermoFisher
722 Scientific), Alexa Fluor 594 donkey anti-goat (Invitrogen by ThermoFisher Scientific) and Alexa Fluor 488
723 donkey anti-rabbit (Invitrogen by ThermoFisher Scientific). Images were collected on a Zeiss Axiovision
724 4.6 wide-field fluorescence microscope at 100X magnification. The same imaging parameters were used
725 for all samples.

726 **Wide-field microscopy analysis**

727 For each strain, 50 or more adjacent and randomly selected nuclei were imaged. A field of nuclei
728 was chosen for analysis based on the DAPI staining pattern. Nuclei were scored as focus positive if there
729 were 3 or more immunostaining foci in a given nucleus. Due to focus crowding in wide-field images, it was
730 not possible to generate reliable focus counts using automated methods. Therefore, focus counts were
731 determined by eye for the experiments reported in Supplemental Figure 8.

732 **One-dimensional gel electrophoresis**

733 One-dimensional gel electrophoresis at the *HIS4:LEU2* meiotic hotspot was performed as follows.
734 15 milliliter sporulation media samples were collected at time points indicated from meiotic cultures.
735 Sodium azide was added to a final concentration of 0.1%. Cells were spun down at 3000 rpm in tabletop
736 clinical centrifuges for 5 minutes, then the supernatant was removed and the pellet was frozen at -20°C.
737 DNA was then purified as described previously [105]. Approximately 2 micrograms DNA per sample was

738 then digested with XhoI restriction enzyme (New England BioLabs) and processed as described
739 previously [105]. Samples were then run on a 0.6% agarose gel at 2V/cm for 24 hours, followed by
740 Southern blotting as described previously [78].

741 **Two-dimensional gel electrophoresis**

742 Two-dimensional gel electrophoresis at the *HIS4:LEU2* meiotic hotspot was performed as
743 previously described [3].

744 **Meiotic two-hybrid analysis**

745 Analysis of Rad51-Dmc1 interaction in meiotic cells was performed using the meiotic two-hybrid
746 method [106]. DNA binding domain constructs were transformed into *MATa* haploid strains DKB6431
747 (*MEI5*⁺) and DKB6429 (*mei5*) and activation domain constructs were transformed into *MATα* haploid
748 strains DKB6430 (*MEI5*⁺) and DKB6428 (*mei5*). Independent transformants were mated to generate the
749 diploid strains used for meiotic two hybrid experiments. 5 ml cultures were grown for 72 hours in synthetic
750 tryptophan leucine dropout media to maintain 2μ plasmids and then transferred to YPD medium at
751 OD₆₀₀=0.2, and then grown for two generations before being transferred to SPS medium overnight, after
752 which sporulation was induced on SPM-1/5COM medium. Recipes for media are as described previously
753 [51]. Samples were prepared for β-galactosidase assays after 6 hours and 18 hours. The plasmids used
754 for the two-hybrid studies were derived from pGAD-C1 [107] for activation domain fusions, and from
755 pCA1 a gift from Scott Keeney [106] for DNA binding domain fusions. Note that this system uses *E. coli*
756 *lexA* as DNA binding domain for hybrid constructs in combination with a *lex-op::lacZ* reporter construct
757 [106]. Plasmid designations and the markers carried by the plasmids were as follows:

758 Dmc1BD=pNRB729 2μ, *TRP1*, *P_{DMC1}-DMC1-lexA*, *ampR*, *ori*; Dmc1AD=pNRB271 2μ, *LEU2*, *P_{ADH}*
759 *GAL4-AD::DMC1*, *ampR*, *ori*; Rad51BD=pNRB727 2μ, *TRP1*, *P_{DMC1}-lexA-Rad51*, *ampR*, *ori*;
760 Rad51AD=pNRB688 2μ, *LEU2*, *P_{ADH}-GAL4-AD::RAD51*, *ampR*, *ori*; ΔBD=pNRB728 2μ, *TRP1*, *P_{DMC1}*
761 *lexA*, *ampR*, *ori*; and ΔAD=pNRB267 2μ, *LEU2*, *P_{ADH}-GAL4*, *ampR*, *ori*. Plasmid sequences are available
762 on request.

763 **Immunofluorescence imaging by stimulation depletion (STED) microscopy**

764 Spreads were stained using a protocol described previously [104] with the following modifications.
765 Spreads were dipped in 0.2% Photo-Flo (Kodak) for 30 seconds, the excess was tapped off, and then the

766 slides were washed in 1X TBS for 5 minutes. Spreads were then blocked with 300 μ L 3% BSA in 1X TBS.
767 Following blocking, spreads were incubated with anti-goat Dmc1 (1:800) and anti-Rabbit RPA (1:1000) for
768 \geq 16 hours at 4°C. Slides were then washed in 1X TBS + 0.05% Triton X-100 for 5 minutes with gentle
769 rocking 7 times. Spreads were incubated with fluorochrome-conjugated secondary antibodies Alexa Fluor
770 594 donkey anti-goat and Alex Fluor 488 donkey anti-rabbit (1:1000) (ThermoFisher Scientific) for 2 hours
771 at 4°C, followed by washes as described. Slides were allowed to dry completely in fume hood, then 35 μ L
772 Vectashield (Vector Laboratories, Inc.) was added, a coverslip was placed atop the slide, and the
773 coverslip was sealed with nail polish.

774 Imaging was conducted on a Leica SP8 3D, 3-color Stimulated Emission Depletion (STED) Laser
775 Scanning Confocal Microscope at the University of Chicago Integrated Light Microscopy Core Facility.
776 The same imaging parameters were used for all strains. Images were deconvolved using Huygens
777 software and applying the same settings for each image. Resolution is reported based on measurements
778 taken from deconvolved images.

779 **STED microscopy analysis**

780 To quantitate the number of foci in each nucleus, the image channels were separated, and each
781 channel image was converted to a binary image in ImageJ. The “Analyze Particles” function was used to
782 obtain information regarding the number of foci in an image, the coordinates of the center of each focus,
783 and the major length of each focus. The same settings were used to analyze all images. Colocalization
784 between Dmc1 and RPA was scored in R using the coordinates given by ImageJ to calculate the distance
785 between a given Dmc1 focus and all RPA foci in the nucleus. A Dmc1 focus was scored as colocalizing
786 with a RPA focus if the nearest RPA focus was less than the length of that Dmc1 focus plus a preset RPA
787 value that was calculated for each strain. The RPA value was calculated based on one half of the
788 average length of all RPA foci in that sample plus one half of two standard deviations of that RPA length.
789 This means that if a given Dmc1 focus is sitting side-by-side with an RPA focus, the distance between it
790 and the center of the nearest RPA focus can be the length of that Dmc1 focus plus one half the average
791 length of all RPA foci in that strain background, plus one half of two standard deviations of the RPA focus
792 lengths. This calculation attempts to take into account the fact that both RPA foci and Dmc1 focus lengths

793 vary from sample to sample. Plots and statistical tests were carried out in R using the ggplot and ggpubr
794 packages.

795 **Meiotic whole cell lysate, SDS-PAGE, and Western blotting**

796 4 milliliters of meiotic culture was collected at the appropriate time point. Trichloroacetic acid
797 was added to a final concentration of 10% weight/volume. Samples were placed in a 60°C water bath for
798 5 minutes, then placed on ice for 5 minutes. Next, samples were spun down at 3000 rotations per minute
799 in a low-speed centrifuge, the supernatant removed by aspiration, and pellet then washed in ddH₂O. The
800 pellet was then re-suspended in 1X-SDS-PAGE (60 mM TrisHCl pH 6.8, 0.05% SDS, 100 mM DTT, 5%
801 glycerol) buffer supplemented with 50 mM sodium PIPES pH 7.5 to the appropriate concentration
802 according to the optical density of cells in the sample. The samples were then boiled for 10 minutes, spun
803 down, and pellets stored at -20°C.

804 A 12% SDS-polyacrylamide gel was prepared, and 30 microliters of each sample was run at
805 120V for 1.5 hours alongside 20 nanograms purified Dmc1 protein. Samples were then transferred to
806 Merck Millipore Limited Immobilon-P Transfer Membrane for 16 hours at 50V at 4°C. The membrane was
807 then blotted using anti-goat Dmc1 (1:1000) primary antibody and an anti-goat HRP-conjugated secondary
808 antibody (1:1000).

809

810 **Acknowledgments**

811 We thank Wolf-Dietrich Heyer for helpful discussions and suggestions. Thanks to Akira Shinohara
812 for the gift of the anti-rabbit RFA2 antibody, and Scott Keeney for the gift of the meiotic two-hybrid strains.
813 We are grateful to Vytas Bindokas and Christine Labno for assistance with STED microscopy. Melissa
814 Castiglione constructed the strains and one of the plasmids used in the two-hybrid analysis. This work
815 was supported by NIGMS grant GM50936 and NCATS grant 1UL1TR002389-01 to DKB. DFR was partly
816 supported by the NIH Genetics & Regulation Training Grant (T32 GM07197).

817

818 **Author Contributions**

819 DFR and DKB jointly conceived the project and planned the experiments. DFR collected and
820 analyzed the data shown in Figures 1-5, Supplemental Figures 1-4 and 6. JTG collected and analyzed
821 the data for Supplemental Figure 5. DKB collected and analyzed the data for Supplemental Figures 7 and
822 8. DFR wrote the original manuscript. DFR and DKB jointly revised the manuscript. DKB was responsible
823 for funding acquisition and project administration.

824

825 **References**

- 826 1. Hunter N. Meiotic Recombination: The Essence of Heredity. Cold Spring Harb Perspect
827 Biol. Cold Spring Harbor Lab; 2015 Oct 28;7(12):a016618–35.
- 828 2. Bishop DK, Park D, Xu L, Kleckner N. *DMC1*: a meiosis-specific yeast homolog of *E. coli*
829 *recA* required for recombination, synaptonemal complex formation, and cell cycle
830 progression. Cell. 1992 May 1;69(3):439–56.
- 831 3. Cloud V, Chan Y-L, Grubb J, Budke B, Bishop DK. Rad51 is an accessory factor for Dmc1-
832 mediated joint molecule formation during meiosis. Science. 2012 Sep 7;337(6099):1222–5.
- 833 4. Symington LS. Mechanism and regulation of DNA end resection in eukaryotes. Critical
834 Reviews in Biochemistry and Molecular Biology. 2016 Apr 20;51(3):195–212.
- 835 5. Bell JC, Kowalczykowski SC. RecA: Regulation and Mechanism of a Molecular Search
836 Engine. Trends Biochem Sci. 2016 Jun;41(6):491–507.
- 837 6. Jinks-Robertson S, Petes TD. High-frequency meiotic gene conversion between repeated
838 genes on nonhomologous chromosomes in yeast. Proc Natl Acad Sci USA. 1985
839 May;82(10):3350–4.
- 840 7. Lichten M, Borts RH, Haber JE. Meiotic gene conversion and crossing over between
841 dispersed homologous sequences occurs frequently in *Saccharomyces cerevisiae*.
842 Genetics. 1987 Feb;115(2):233–46.
- 843 8. Goldman AS, Lichten M. The efficiency of meiotic recombination between dispersed
844 sequences in *Saccharomyces cerevisiae* depends upon their chromosomal location.
845 Genetics. 1996 Sep;144(1):43–55.
- 846 9. Grushcow JM, Holzen TM, Park KJ, Weinert T, Lichten M, Bishop DK. *Saccharomyces*
847 *cerevisiae* checkpoint genes *MEC1*, *RAD17* and *RAD24* are required for normal meiotic
848 recombination partner choice. Genetics. 1999 Oct;153(2):607–20.
- 849 10. Schwacha A, Kleckner N. Identification of joint molecules that form frequently between
850 homologs but rarely between sister chromatids during yeast meiosis. Cell. 1994 Jan
851 14;76(1):51–63.
- 852 11. Brown MS, Bishop DK. DNA Strand Exchange and RecA Homologs in Meiosis. Cold Spring
853 Harb Perspect Biol. 2015 Jan 5;7(1):a016659–31.
- 854 12. Wright WD, Shah SS, Heyer W-D. Homologous recombination and the repair of DNA
855 double-strand breaks. J Biol Chem. 2018 Jul 6;293(27):10524–35.
- 856 13. Heyer W-D. Regulation of recombination and genomic maintenance. Cold Spring Harb
857 Perspect Biol. 2015 Aug 3;7(8):a016501.
- 858 14. Krejci L, Altmannova V, Spirek M, Zhao X. Homologous recombination and its regulation.
859 Nucleic Acids Res. 2012 Jul;40(13):5795–818.
- 860 15. Kowalczykowski SC. An Overview of the Molecular Mechanisms of Recombinational DNA
861 Repair. Cold Spring Harb Perspect Biol. 2015 Nov 2;7(11).
- 862 16. Krejci L, Van Komen S, Li Y, Villemain J, Reddy MS, Klein H, et al. DNA helicase Srs2
863 disrupts the Rad51 presynaptic filament. Nature. 2003 May 15;423(6937):305–9.

- 864 17. Veaute X, Jeusset J, Soustelle C, Kowalczykowski SC, Le Cam E, Fabre F. The Srs2
865 helicase prevents recombination by disrupting Rad51 nucleoprotein filaments. *Nature*. 2003
866 May 15;423(6937):309–12.
- 867 18. Veaute X, Delmas S, Selva M, Jeusset J, Le Cam E, Matic I, et al. UvrD helicase, unlike
868 Rep helicase, dismantles RecA nucleoprotein filaments in *Escherichia coli*. *EMBO J*. 2005
869 Jan 12;24(1):180–9.
- 870 19. Petrova V, Chen SH, Molzberger ET, Tomko E, Chitteni-Pattu S, Jia H, et al. Active
871 displacement of RecA filaments by UvrD translocase activity. *Nucleic Acids Res*. 2015 Apr
872 30;43(8):4133–49.
- 873 20. Sasanuma H, Furihata Y, Shinohara M, Shinohara A. Remodeling of the Rad51 DNA
874 strand-exchange protein by the Srs2 helicase. *Genetics*. 2013 Aug;194(4):859–72.
- 875 21. Crickard JB, Kaniecki K, Kwon Y, Sung P, Greene EC. Meiosis-specific recombinase Dmc1
876 is a potent inhibitor of the Srs2 antirecombinase. *Proc Natl Acad Sci USA*. 2018 Oct
877 23;115(43):E10041–8.
- 878 22. Bishop DK, Ear U, Bhattacharyya A, Calderone C, Beckett M, Weichselbaum RR, et al.
879 Xrcc3 is required for assembly of Rad51 complexes *in vivo*. *Journal of Biological Chemistry*.
880 1998 Aug 21;273(34):21482–8.
- 881 23. Gasior SL, Olivares H, Ear U, Hari DM, Weichselbaum R, Bishop DK. Assembly of RecA-
882 like recombinases: distinct roles for mediator proteins in mitosis and meiosis. *Proc Natl*
883 *Acad Sci USA*. 2001 Jul 17;98(15):8411–8.
- 884 24. Haaf T, Golub EI, Reddy G, Radding CM, Ward DC. Nuclear foci of mammalian Rad51
885 recombination protein in somatic cells after DNA damage and its localization in
886 synaptonemal complexes. *Proc Natl Acad Sci USA*. 1995 Mar 14;92(6):2298–302.
- 887 25. Gataulin DV, Carey JN, Li J, Shah P, Grubb JT, Bishop DK. The ATPase activity of *E. coli*
888 RecA prevents accumulation of toxic complexes formed by erroneous binding to
889 undamaged double stranded DNA. *Nucleic Acids Res*. 2018 Oct 12;46(18):9510–23.
- 890 26. Brown MS, Grubb J, Zhang A, Rust MJ, Bishop DK. Small Rad51 and Dmc1 Complexes
891 Often Co-occupy Both Ends of a Meiotic DNA Double Strand Break. *PLoS Genet*. 2015
892 Dec;11(12):e1005653.
- 893 27. Egelman EH, Stasiak A. Structure of helical RecA-DNA complexes. Complexes formed in
894 the presence of ATP-gamma-S or ATP. *J Mol Biol*. 1986 Oct 20;191(4):677–97.
- 895 28. Zakharyevich K, Ma Y, Tang S, Hwang PY-H, Boiteux S, Hunter N. Temporally and
896 biochemically distinct activities of Exo1 during meiosis: double-strand-break resection and
897 resolution of double-Holliday junctions. *Molecular Cell*. 2010 Dec 22;40(6):1001–15.
- 898 29. Menetski JP, Bear DG, Kowalczykowski SC. Stable DNA heteroduplex formation catalyzed
899 by the *Escherichia coli* RecA protein in the absence of ATP hydrolysis. *Proc Natl Acad Sci*
900 *USA*. 1990 Jan;87(1):21–5.
- 901 30. Rosselli W, Stasiak A. Energetics of RecA-mediated recombination reactions. Without ATP
902 hydrolysis RecA can mediate polar strand exchange but is unable to recycle. *J Mol Biol*.
903 1990 Nov 20;216(2):335–52.
- 904 31. Sung P, Stratton SA. Yeast Rad51 recombinase mediates polar DNA strand exchange in

- 905 the absence of ATP hydrolysis. *Journal of Biological Chemistry*. 1996 Nov
906 8;271(45):27983–6.
- 907 32. Campbell MJ, Davis RW. Toxic mutations in the *recA* gene of *E. coli* prevent proper
908 chromosome segregation. *J Mol Biol*. 1999 Feb 19;286(2):417–35.
- 909 33. Stasiak A, Egelman EH. Visualization of recombination intermediates. Kucherlapati R, Smith
910 GR, editors. *Genetic Recombination*. Washington: American Society for Microbiology; 1988.
911 p. 265-308.
- 912 34. Sung P. Catalysis of ATP-dependent homologous DNA pairing and strand exchange by
913 yeast RAD51 protein. *Science*. 1994 Aug 26;265(5176):1241–3.
- 914 35. Zaitseva EM, Zaitsev EN, Kowalczykowski SC. The DNA binding properties of
915 *Saccharomyces cerevisiae* Rad51 protein. *Journal of Biological Chemistry*. 1999 Jan
916 29;274(5):2907–15.
- 917 36. Hong EL, Shinohara A, Bishop DK. *Saccharomyces cerevisiae* Dmc1 protein promotes
918 renaturation of single-strand DNA (ssDNA) and assimilation of ssDNA into homologous
919 super-coiled duplex DNA. *Journal of Biological Chemistry*. 2001 Nov 9;276(45):41906–12.
- 920 37. Solinger JA, Kiiianitsa K, Heyer W-D. Rad54, a Swi2/Snf2-like recombinational repair
921 protein, disassembles Rad51:dsDNA filaments. *Molecular Cell*. 2002 Nov;10(5):1175–88.
- 922 38. Sheridan SD, Yu X, Roth R, Heuser JE, Sehorn MG, Sung P, et al. A comparative analysis
923 of Dmc1 and Rad51 nucleoprotein filaments. *Nucleic Acids Res*. 2008 Jul;36(12):4057–66.
- 924 39. Li X, Heyer W-D. RAD54 controls access to the invading 3'-OH end after RAD51-mediated
925 DNA strand invasion in homologous recombination in *Saccharomyces cerevisiae*. *Nucleic
926 Acids Res*. 2009 Feb;37(2):638–46.
- 927 40. Chi P, Kwon Y, Seong C, Epshtein A, Lam I, Sung P, et al. Yeast recombination factor
928 Rdh54 functionally interacts with the Rad51 recombinase and catalyzes Rad51 removal
929 from DNA. *Journal of Biological Chemistry*. 2006 Sep 8;281(36):26268–79.
- 930 41. Holzen TM, Shah PP, Olivares HA, Bishop DK. Tid1/Rdh54 promotes dissociation of Dmc1
931 from nonrecombinogenic sites on meiotic chromatin. *Genes Dev*. 2006 Sep
932 15;20(18):2593–604.
- 933 42. Shah PP, Zheng X, Epshtein A, Carey JN, Bishop DK, Klein HL. Swi2/Snf2-related
934 translocases prevent accumulation of toxic Rad51 complexes during mitotic growth.
935 *Molecular Cell*. 2010 Sep 24;39(6):862–72.
- 936 43. Mason JM, Dusad K, Wright WD, Grubb J, Budke B, Heyer W-D, et al. RAD54 family
937 translocases counter genotoxic effects of RAD51 in human tumor cells. *Nucleic Acids Res*.
938 2015 Mar 31;43(6):3180–96.
- 939 44. Hilario J, Amitani I, Baskin RJ, Kowalczykowski SC. Direct imaging of human Rad51
940 nucleoprotein dynamics on individual DNA molecules. *Proc Natl Acad Sci USA*. 2009 Jan
941 13;106(2):361–8.
- 942 45. Morgan EA, Shah N, Symington LS. The requirement for ATP hydrolysis by *Saccharomyces
943 cerevisiae* Rad51 is bypassed by mating-type heterozygosity or *RAD54* in high copy. *Mol
944 Cell Biol*. 2002 Sep;22(18):6336–43.

- 945 46. Fung CW, Fortin GS, Peterson SE, Symington LS. The *rad51-K191R* ATPase-defective
946 mutant is impaired for presynaptic filament formation. *Mol Cell Biol.* 2006 Dec;26(24):9544–
947 54.
- 948 47. Li X, Zhang X-P, Solinger JA, Kiiianitsa K, Yu X, Egelman EH, et al. Rad51 and Rad54
949 ATPase activities are both required to modulate Rad51-dsDNA filament dynamics. *Nucleic*
950 *Acids Res.* 2007;35(12):4124–40.
- 951 48. Conway AB, Lynch TW, Zhang Y, Fortin GS, Fung CW, Symington LS, et al. Crystal
952 structure of a Rad51 filament. *Nat Struct Mol Biol.* 2004 Aug;11(8):791–6.
- 953 49. Galkin VE, Wu Y, Zhang X-P, Qian X, He Y, Yu X, et al. The Rad51/RadA N-terminal
954 domain activates nucleoprotein filament ATPase activity. *Structure.* 2006 Jun;14(6):983–92.
- 955 50. Chan Y-L, Zhang A, Weissman BP, Bishop DK. RPA resolves conflicting activities of
956 accessory proteins during reconstitution of Dmc1-mediated meiotic recombination. *Nucleic*
957 *Acids Res.* 2019 Jan 25;47(2):747–61.
- 958 51. Bishop DK. RecA homologs Dmc1 and Rad51 interact to form multiple nuclear complexes
959 prior to meiotic chromosome synapsis. *Cell.* 1994 Dec 16;79(6):1081–92.
- 960 52. Hayase A, Takagi M, Miyazaki T, Oshiumi H, Shinohara M, Shinohara A. A Protein Complex
961 Containing Mei5 and Sae3 Promotes the Assembly of the Meiosis-Specific RecA Homolog
962 Dmc1. *Cell.* 2004 Dec;119(7):927–40.
- 963 53. Tsubouchi H, Roeder GS. The budding yeast Mei5 and Sae3 proteins act together with
964 Dmc1 during meiotic recombination. *Genetics.* 2004 Nov;168(3):1219–30.
- 965 54. Zierhut C, Berlinger M, Rupp C, Shinohara A, Klein F. Mnd1 Is Required for Meiotic
966 Interhomolog Repair. *Current Biology.* 2004 May;14(9):752–62.
- 967 55. Henry JM, Camahort R, Rice DA, Florens L, Swanson SK, Washburn MP, et al. Mnd1/Hop2
968 facilitates Dmc1-dependent interhomolog crossover formation in meiosis of budding yeast.
969 *Mol Cell Biol.* 2006 Apr;26(8):2913–23.
- 970 56. Argunhan B, Murayama Y, Iwasaki H. The differentiated and conserved roles of Swi5-Sfr1 in
971 homologous recombination. *FEBS Lett.* 2017 May 8;591(14):2035–47.
- 972 57. Haruta N, Kurokawa Y, Murayama Y, Akamatsu Y, Unzai S, Tsutsui Y, et al. The Swi5-Sfr1
973 complex stimulates Rhp51/Rad51- and Dmc1-mediated DNA strand exchange *in vitro*. *Nat*
974 *Struct Mol Biol.* 2006 Sep;13(9):823–30.
- 975 58. Yuan J, Chen J. The role of the human SWI5-MEI5 complex in homologous recombination
976 repair. *J Biol Chem.* 2011 Mar 18;286(11):9888–93.
- 977 59. Su G-C, Chung C-I, Liao C-Y, Lin S-W, Tsai C-T, Huang T, et al. Enhancement of ADP
978 release from the RAD51 presynaptic filament by the SWI5-SFR1 complex. *Nucleic Acids*
979 *Res.* 2014 Jan;42(1):349–58.
- 980 60. Ferrari SR, Grubb J, Bishop DK. The Mei5-Sae3 Protein Complex Mediates Dmc1 Activity in
981 *Saccharomyces cerevisiae*. *Journal of Biological Chemistry.* 2009 Apr 24;284(18):11766–
982 70.
- 983 61. Bugreev DV, Mazin AV. Ca²⁺ activates human homologous recombination protein Rad51 by
984 modulating its ATPase activity. *Proc Natl Acad Sci USA.* 2004 Jul 6;101(27):9988–93.

- 985 62. Lu C-H, Yeh H-Y, Su G-C, Ito K, Kurokawa Y, Iwasaki H, et al. Swi5-Sfr1 stimulates Rad51
986 recombinase filament assembly by modulating Rad51 dissociation. Proc Natl Acad Sci USA.
987 2018 Oct 23;115(43):E10059–68.
- 988 63. McKee AH, Kleckner N. Mutations in *Saccharomyces cerevisiae* that block meiotic prophase
989 chromosome metabolism and confer cell cycle arrest at pachytene identify two new meiosis-
990 specific genes *SAE1* and *SAE3*. Genetics. 1997 Jul;146(3):817–34.
- 991 64. Akamatsu Y, Tsutsui Y, Morishita T, Siddique MSP, Kurokawa Y, Ikeguchi M, et al. Fission
992 yeast Swi5/Sfr1 and Rhp55/Rhp57 differentially regulate Rhp51-dependent recombination
993 outcomes. EMBO J. 2007 Mar 7;26(5):1352–62.
- 994 65. Akamatsu Y, Jasin M. Role for the mammalian Swi5-Sfr1 complex in DNA strand break
995 repair through homologous recombination. PLoS Genet. 2010 Oct 14;6(10):e1001160.
- 996 66. Tsubouchi H, Roeder GS. Budding yeast Hed1 down-regulates the mitotic recombination
997 machinery when meiotic recombination is impaired. Genes Dev. 2006 Jul 1;20(13):1766–75.
- 998 67. Busygina V, Sehorn MG, Shi IY, Tsubouchi H, Roeder GS, Sung P. Hed1 regulates Rad51-
999 mediated recombination via a novel mechanism. Genes Dev. 2008 Mar 15;22(6):786–95.
- 1000 68. Shinohara A, Gasior S, Ogawa T, Kleckner N, Bishop DK. *Saccharomyces cerevisiae* *recA*
1001 homologues *RAD51* and *DMC1* have both distinct and overlapping roles in meiotic
1002 recombination. Genes Cells. 1997 Oct;2(10):615–29.
- 1003 69. Schwacha A, Kleckner N. Interhomolog bias during meiotic recombination: meiotic functions
1004 promote a highly differentiated interhomolog-only pathway. Cell. 1997 Sep 19;90(6):1123–
1005 35.
- 1006 70. Shinohara A, Ogawa H, Ogawa T. Rad51 protein involved in repair and recombination in *S.*
1007 *cerevisiae* is a RecA-like protein. Cell. 1992 May 1;69(3):457–70.
- 1008 71. Campbell MJ, Davis RW. On the *in vivo* function of the RecA ATPase. J Mol Biol. 1999 Feb
1009 19;286(2):437–45.
- 1010 72. Fortin GS, Symington LS. Mutations in yeast Rad51 that partially bypass the requirement for
1011 Rad55 and Rad57 in DNA repair by increasing the stability of Rad51-DNA complexes.
1012 EMBO J. 2002 Jun 17;21(12):3160–70.
- 1013 73. Keeney S, Giroux CN, Kleckner N. Meiosis-specific DNA double-strand breaks are
1014 catalyzed by Spo11, a member of a widely conserved protein family. Cell. 1997 Feb
1015 7;88(3):375–84.
- 1016 74. Gasior SL, Wong AK, Kora Y, Shinohara A, Bishop DK. Rad52 associates with RPA and
1017 functions with Rad55 and Rad57 to assemble meiotic recombination complexes. Genes
1018 Dev. Cold Spring Harbor Lab; 1998 Jul 15;12(14):2208–21.
- 1019 75. Hunter N, Kleckner N. The single-end invasion: an asymmetric intermediate at the double-
1020 strand break to double-Holliday junction transition of meiotic recombination. Cell. 2001 Jul
1021 13;106(1):59–70.
- 1022 76. Cao L, Alani E, Kleckner N. A pathway for generation and processing of double-strand
1023 breaks during meiotic recombination in *S. cerevisiae*. Cell. 1990 Jun 15;61(6):1089–101.
- 1024 77. Shinohara M, Shinohara A. Multiple pathways suppress non-allelic homologous

- 1025 recombination during meiosis in *Saccharomyces cerevisiae*. PLoS ONE. 2013;8(4):e63144.
- 1026 78. Oh SD, Jessop L, Lao JP, Allers T, Lichten M, Hunter N. Stabilization and electrophoretic
1027 analysis of meiotic recombination intermediates in *Saccharomyces cerevisiae*. Methods Mol
1028 Biol. 2009;557(Chapter 14):209–34.
- 1029 79. Hong S, Sung Y, Yu M, Lee M, Kleckner N, Kim KP. The Logic and Mechanism of
1030 Homologous Recombination Partner Choice. Molecular Cell. 2013 Aug 22;51(4):440–53.
- 1031 80. Lao JP, Cloud V, Huang C-C, Grubb J, Thacker D, Lee C-Y, et al. Meiotic Crossover Control
1032 by Concerted Action of Rad51-Dmc1 in Homolog Template Bias and Robust Homeostatic
1033 Regulation. PLoS Genet. 2013 Dec 19;9(12):e1003978.
- 1034 81. Dresser ME, Ewing DJ, Conrad MN, Dominguez AM, Barstead R, Jiang H, et al. *DMC1*
1035 functions in a *Saccharomyces cerevisiae* meiotic pathway that is largely independent of the
1036 *RAD51* pathway. Genetics. 1997 Oct;147(2):533–44.
- 1037 82. Bishop DK. Rad51, the lead in mitotic recombinational DNA repair, plays a supporting role
1038 in budding yeast meiosis. Cell Cycle. 2012 Nov 15;11(22):4105–6.
- 1039 83. Masson JY, Davies AA, Hajibagheri N, Van Dyck E, Benson FE, Stasiak AZ, et al. The
1040 meiosis-specific recombinase hDmc1 forms ring structures and interacts with hRad51.
1041 EMBO J. 1999 Nov 15;18(22):6552–60.
- 1042 84. Tarsounas M, Morita T, Pearlman RE, Moens PB. RAD51 and DMC1 form mixed
1043 complexes associated with mouse meiotic chromosome cores and synaptonemal
1044 complexes. J Cell Biol. 1999 Oct 18;147(2):207–20.
- 1045 85. Siaud N, Dray E, Gy I, Gérard E, Takvorian N, Doutriaux M-P. Brca2 is involved in meiosis
1046 in *Arabidopsis thaliana* as suggested by its interaction with Dmc1. EMBO J. 2004 Mar
1047 24;23(6):1392–401.
- 1048 86. Shinohara M, Gasior SL, Bishop DK, Shinohara A. Tid1/Rdh54 promotes colocalization of
1049 Rad51 and Dmc1 during meiotic recombination. Proc Natl Acad Sci USA. 2000 Sep
1050 26;97(20):10814–9.
- 1051 87. Shan Q, Bork JM, Webb BL, Inman RB, Cox MM. RecA protein filaments: end-dependent
1052 dissociation from ssDNA and stabilization by RecO and RecR proteins. J Mol Biol. 1997 Feb
1053 7;265(5):519–40.
- 1054 88. Sung P. Yeast Rad55 and Rad57 proteins form a heterodimer that functions with replication
1055 protein A to promote DNA strand exchange by Rad51 recombinase. Genes Dev. 1997 May
1056 1;11(9):1111–21.
- 1057 89. Liu J, Renault L, Veaute X, Fabre F, Stahlberg H, Heyer W-D. Rad51 paralogs Rad55-
1058 Rad57 balance the anti-recombinase Srs2 in Rad51 filament formation. Nature. 2011 Oct
1059 23;479(7372):245–8.
- 1060 90. Shinohara M, Shita-Yamaguchi E, Buerstedde JM, Shinagawa H, Ogawa H, Shinohara A.
1061 Characterization of the roles of the *Saccharomyces cerevisiae* *RAD54* gene and a
1062 homologue of *RAD54*, *RDH54/TID1*, in mitosis and meiosis. Genetics. 1997
1063 Dec;147(4):1545–56.
- 1064 91. Oh SD, Lao JP, Hwang PY-H, Taylor AF, Smith GR, Hunter N. BLM ortholog, Sgs1,
1065 prevents aberrant crossing-over by suppressing formation of multi-chromatid joint

- 1066 molecules. *Cell*. 2007 Jul 27;130(2):259–72.
- 1067 92. Kaur H, De Muyt A, Lichten M. Top3-Rmi1 DNA single-strand decatenase is integral to the
1068 formation and resolution of meiotic recombination intermediates. *Molecular Cell*. 2015 Feb
1069 19;57(4):583–94.
- 1070 93. Tang S, Wu MKY, Zhang R, Hunter N. Pervasive and essential roles of the Top3-Rmi1
1071 decatenase orchestrate recombination and facilitate chromosome segregation in meiosis.
1072 *Molecular Cell*. 2015 Feb 19;57(4):607–21.
- 1073 94. Cejka P, Plank JL, Bachrati CZ, Hickson ID, Kowalczykowski SC. Rmi1 stimulates
1074 decatenation of double Holliday junctions during dissolution by Sgs1-Top3. *Nat Struct Mol*
1075 *Biol*. 2010 Nov;17(11):1377–82.
- 1076 95. Fasching CL, Cejka P, Kowalczykowski SC, Heyer W-D. Top3-Rmi1 dissolve Rad51-
1077 mediated D-loops by a topoisomerase-based mechanism. *Molecular Cell*. 2015 Feb
1078 19;57(4):595–606.
- 1079 96. Piazza A, Shah SS, Wright WD, Gore SK, Koszul R, Heyer W-D. Dynamic Processing of
1080 Displacement Loops during Recombinational DNA Repair. *Molecular Cell*. 2019 Mar
1081 21;73(6):1255–1266.e4.
- 1082 97. Piazza A, Wright WD, Heyer W-D. Multi-invasions Are Recombination Byproducts that
1083 Induce Chromosomal Rearrangements. *Cell*. 2017 Aug 10;170(4):760–773.e15.
- 1084 98. Piazza A, Heyer W-D. Multi-Invasion-Induced Rearrangements as a Pathway for
1085 Physiological and Pathological Recombination. *Bioessays*. 2018 May;40(5):e1700249.
- 1086 99. Oh SD, Lao JP, Taylor AF, Smith GR, Hunter N. RecQ helicase, Sgs1, and XPF family
1087 endonuclease, Mus81-Mms4, resolve aberrant joint molecules during meiotic
1088 recombination. *Molecular Cell*. 2008 Aug 8;31(3):324–36.
- 1089 100. Jessop L, Lichten M. Mus81/Mms4 endonuclease and Sgs1 helicase collaborate to ensure
1090 proper recombination intermediate metabolism during meiosis. *Molecular Cell*. 2008 Aug
1091 8;31(3):313–23.
- 1092 101. De Muyt A, Jessop L, Kolar E, Sourirajan A, Chen J, Dayani Y, et al. BLM helicase ortholog
1093 Sgs1 is a central regulator of meiotic recombination intermediate metabolism. *Molecular*
1094 *Cell*. 2012 Apr 13;46(1):43–53.
- 1095 102. Forget AL, Kowalczykowski SC. Single-molecule imaging of DNA pairing by RecA reveals a
1096 three-dimensional homology search. *Nature*. 2012 Feb 5;482(7385):423–7.
- 1097 103. Wright WD, Heyer W-D. Rad54 functions as a heteroduplex DNA pump modulated by its
1098 DNA substrates and Rad51 during D-loop formation. *Molecular Cell*. 2014 Feb 6;53(3):420–
1099 32.
- 1100 104. Grubb J, Brown MS, Bishop DK. Surface Spreading and Immunostaining of Yeast
1101 Chromosomes. *J Vis Exp*. 2015 Aug 9;(102):e53081.
- 1102 105. Lao JP, Tang S, Hunter N. Native/Denaturing two-dimensional DNA electrophoresis and its
1103 application to the analysis of recombination intermediates. *Methods Mol Biol*. 2013;1054(Pt
1104 2):105–20.
- 1105 106. Arora C, Kee K, Maleki S, Keeney S. Antiviral protein Ski8 is a direct partner of Spo11 in

- 1106 meiotic DNA break formation, independent of its cytoplasmic role in RNA metabolism.
1107 Molecular Cell. 2004 Feb 27;13(4):549–59.
- 1108 107. James P, Halladay J, Craig EA. Genomic Libraries and a Host Strain Designed for Highly
1109 Efficient Two-Hybrid Selection in Yeast. Genetics. 1996 Dec;144(4):1425–36.
- 1110

1111 **Figure Captions**

1112

1113 **Table 1.** Spore viabilities for strains in study. p-values are reported for z-scores.

1114 Comparison for single mutants is to wild-type. Comparison for double mutants is to each of the single
1115 mutants; the largest p-value is reported. Comparison for heterozygotes is to homozygotes. N.A. = not
1116 applicable; for samples that do not meet the success/failure condition for z-scores and wild-type to itself.
1117 Strains used in experiments in the order in which they appear in table, top to bottom: DKB3698,
1118 DKB6320, DKB3710, DKB3689, DKB2526, DKB6342, DKB6299, DKB6300, DKB6539, DKB6540,
1119 DKB6393, DKB6400, DKB6583, DKB6412, DKB6413, DKB6525, DKB6619, DKB6406, DKB6407.

1120

1121 **Figure 1.** *dmc1-E157D* bypasses *mei5*, *rad51* with respect to focus formation.

1122 (a, c) Representative widefield microscopy imaging of spread meiotic nuclei are shown for each strain.
1123 Scale bars represent 1 μ m. (b, d) Quantitation. Nuclei were scored as focus positive if they contained
1124 three or more foci of a given type. Dmc1 (green), Rad51 or RPA (red). (e) Quantitation of *spo11* strains
1125 and controls at 4 hours. Strains used in experiments in the order in which they appear in figure, top to
1126 bottom: DKB3698, DKB6320, DKB6342, DKB6300, DKB3710, DKB6393, DKB6412.

1127

1128 **Figure 2.** *dmc1-E157D* bypasses *mei5* but not *rad51* with respect to CO formation.

1129 (a) 1D XhoI gels at the *HIS4::LEU2* hotspot from meiotic time course experiments (b) Quantitation of 1D
1130 gels shown in (a); black – wild-type, light blue – *mei5*, purple – *rad51*, red – *dmc1-E157D*, gray – *dmc1-*
1131 *E157D mei5*, green – *dmc1-E157D rad51*, yellow – *dmc1-E157D mei5 rad51* and meiotic progression
1132 data for each strain. For each time point, ≥ 50 cells were scored. Strains used in experiments in the order
1133 in which they appear in figure, right to left: DKB3698, DKB6320, DKB3710, DKB6342, DKB6300,
1134 DKB6393, DKB6412.

1135

1136 **Figure 3.** Recombination in *dmc1-E157D* is abnormal and dependent on Rad51, with little affect of Mei5-
1137 Sae3.

1138 (a) 2D gels at the *HIS4::LEU2* hotspot from meiotic time course experiments. Representative images
1139 were chosen according to the time at which total JMs peaks for each sample (wild-type, 6 hours; *mei5*, 8
1140 hours; *dmc1-E157D*, 8 hours; *dmc1-E157D mei5*, 7 hours) (b) 2D gel quantitation; black – wild-type, light
1141 blue – *mei5*, red – *dmc1-E157D*, gray – *dmc1-E157D mei5*. (c) 2D gels. Representative images were
1142 chosen according to the time at which total JMs peaks for each sample (*rad51*, 6 hours; *dmc1-E157D*, 6
1143 hours; *dmc1-E157D rad51*, 7.5 hours; *dmc1-E157D mei5 rad51*, 6 hours) (d) 2D gel quantitation; black –
1144 wild-type, light purple – *rad51*, red – *dmc1-E157D*, green – *dmc1-E157D rad51*, yellow – *dmc1-E157D*
1145 *mei5 rad51*. Strains used in experiments in the order in which they appear in figure, right to left and top to
1146 bottom: DKB3698, DKB6320, DKB6342, DKB6300, DKB3710, DKB6393, DKB6412.

1147

1148 **Figure 4.** Super-resolution imaging shows abnormalities in RPA, Dmc1 foci in mutants.

1149 (a) Representative STED microscopy imaging of spread meiotic nuclei are shown for each strain. Scale
1150 bars represent 1 μ m; scale bars in inset represent 0.1 μ m. For *dmc1-E157D mei5*, time point was taken at

1151 5 hours in sporulation media; for all other strains, time point was taken at 4.5 hours. (b) Quantitation of
1152 foci counts for Dmc1, RPA, is shown for each strain. For each strain, 13 randomly selected nuclei were
1153 quantitated. (c) Quantitation of RPA and Dmc1 foci lengths is shown for each strain. (d) Quantitation of
1154 Dmc1 foci lengths colocalizing with RPA is shown for the strains indicated. Strains used in this
1155 experiment in the order in which they appear in figure, top to bottom: DKB3698, DKB3710, DKB6342,
1156 DKB6300, DKB6393, DKB6412.

1157

1158 **Figure 5.** Model for regulation of filament length *in vivo*.

1159

1160 **Supplemental Figure 1.** *DMC1* expression for wild-type, *dmc1-E157D*.

1161 Left column, W. blot against Dmc1 for 5 μ L sample prepared from meiotic yeast cultures at 6 hours as
1162 described in Methods Section for each strain. Control column is 20 ng purified Dmc1 protein that was run
1163 in parallel with sample and used to quantitate blots. Sample concentration is estimated concentration in
1164 comparison to 20 ng purified Dmc1 protein. Similar results were obtained from an independent meiotic
1165 time course. Strains used in this experiment in the order in which they appear in figure, top to bottom:
1166 DKB3698, DKB6342.

1167

1168 **Supplemental Figure 2.** *spo11* suppresses the meiotic progression defect associated with *dmc1-E157D*.

1169 Meiotic progression data for strains indicated. For each time point, ≥ 50 cells were scored. Strains used in
1170 this experiment in the order in which they appear in figure, top to bottom: DKB3698, DKB2123, DKB6342,
1171 DKB6419, DKB6425.

1172

1173 **Supplemental Figure 3.** An independently derived diploid strain (DKB6413) corresponding to the *dmc1-*
1174 *E157D mei5 rad51* genotype gives the same result as shown in Figure 3.

1175 Wild-type and *dmc1-E157D* samples were prepared in parallel as controls. (a) 2D gels gels at the
1176 *HIS4::LEU2* hotspot from meiotic time course experiments. Representative images were chosen
1177 according to the time at which total JMs peaks for each sample. From left to right: wild-type (5h), *dmc1-*
1178 *E157D* (6h), *dmc1-E157D mei5 rad51* (7h). (b) 2D gel quantitation; black – wild-type, red – *dmc1-E157D*,
1179 yellow – *dmc1-E157D mei5 rad51*. Strains used in this experiment in the order in which they appear in
1180 figure, right to left: DKB3698, DKB6342, DKB6413.

1181

1182 **Supplemental Figure 4.** The defects associated with *dmc1-E157D rad51* are independent of Rad51's
1183 catalytic activity.

1184 (a) 2D gels gels at the *HIS4::LEU2* hotspot from meiotic time course experiments. Representative images
1185 were chosen according to the time at which total JMs peaks for each sample. From left to right: wild-type
1186 (6h), *rad51-II3A* (6h), *dmc1-E157D* (6h), *dmc1-E157D rad51-II3A* (6h). (b) 2D gel quantitation; black –
1187 wild-type, gray – *rad51-II3A*, red – *dmc1-E157D*, dark blue – *dmc1-E157D rad51-II3A*. Strains used in this
1188 experiment in the order in which they appear in figure, right to left: DKB3698, DKB3689, DKB6342,
1189 DKB6400.

1190

1191 **Supplemental Figure 5.** Meiotic two-hybrid analysis detects a weak interaction between Rad51 and
1192 Dmc1 that is independent of Mei5.

1193 (a) All interactions examined are plotted. (b) Subset of the same data shown in (a) to facilitate comparison
1194 of measurements of the Rad51-Dmc1 interaction with empty vector controls. Δ BD and Δ AD represent the
1195 empty vectors. Strains used in this experiment: DKB6501, DKB6503, DKB6508, DKB6509, DKB6513,
1196 DKB6515.

1197

1198 **Supplemental Figure 6.** Super-resolution imaging resolves closely spaced foci, but elongated foci still
1199 form in *spo11 dmc1-E157D*.

1200 (a) Spread meiotic nuclei prepared from a *dmc1-E157D mei5* 5 hour sample imaged using confocal and
1201 STED microscopy methods. (b) STED imaging of a *spo11 dmc1-E157D* spread meiotic nuclei at 5 hours.
1202 For both, scale bar represents 1 micrometer. Red, RPA, green, Dmc1. Strains used in this experiment:
1203 DKB630, DKB6419.

1204

1205 **Supplemental Figure 7.** *dmc1-E157D rdh54* is more defective in meiotic progression than either of the
1206 single mutants, *dmc1-E157D* and *rdh54*.

1207 Meiotic progression data for strains indicated. For each time point, ≥ 100 cells were scored. Strains used
1208 in this experiment in the order in which they appear in figure, top to bottom: DKB2526, DKB6342,
1209 DKB6583.

1210

1211 **Supplemental Figure 8.** DSB-independent Dmc1-WT focus formation does not require Mei5.

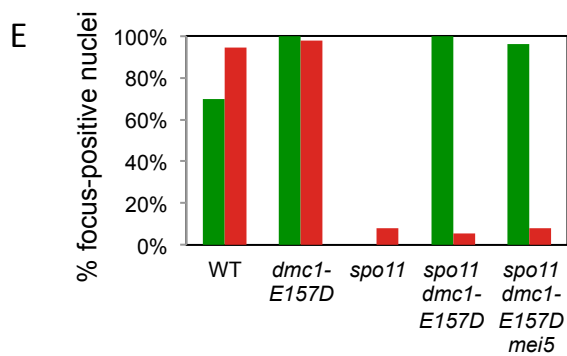
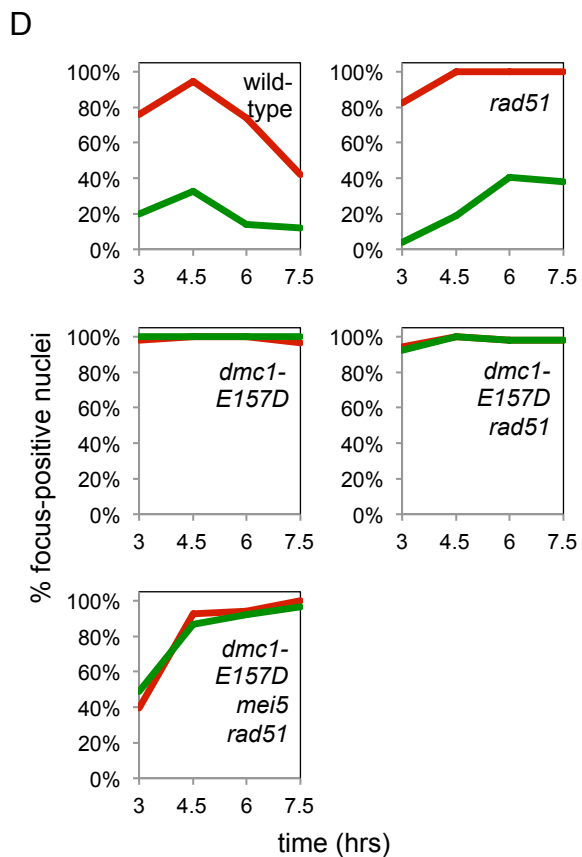
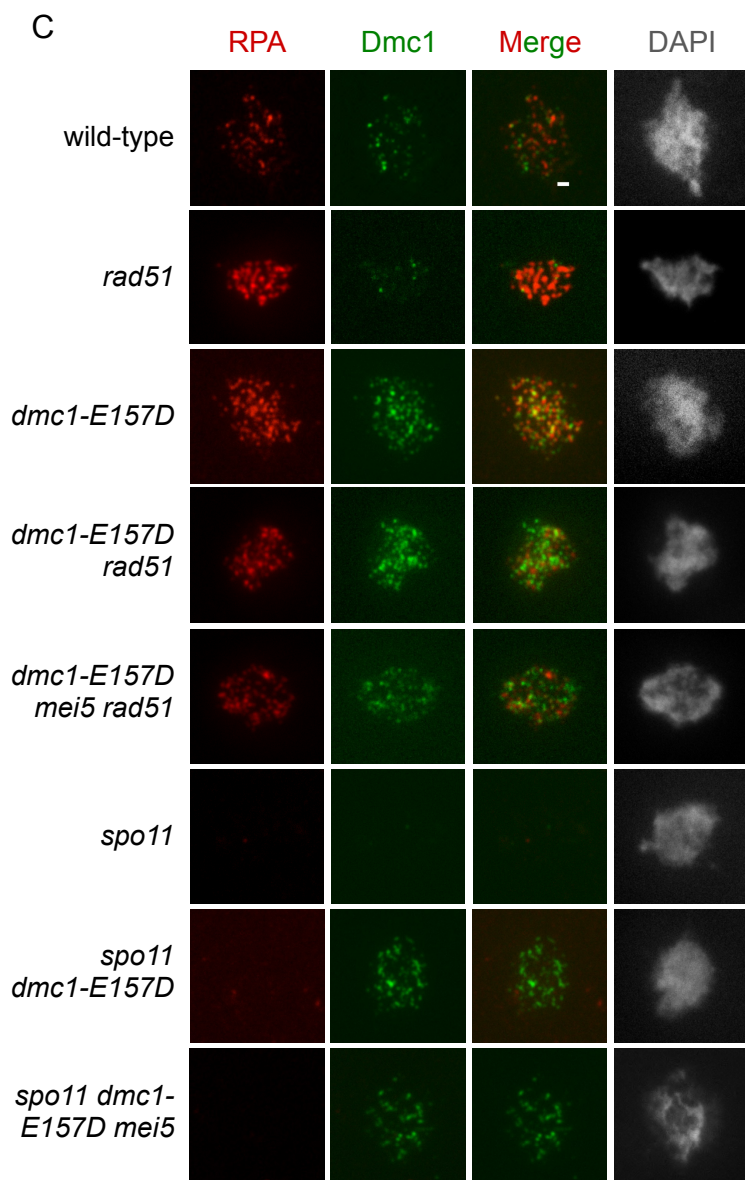
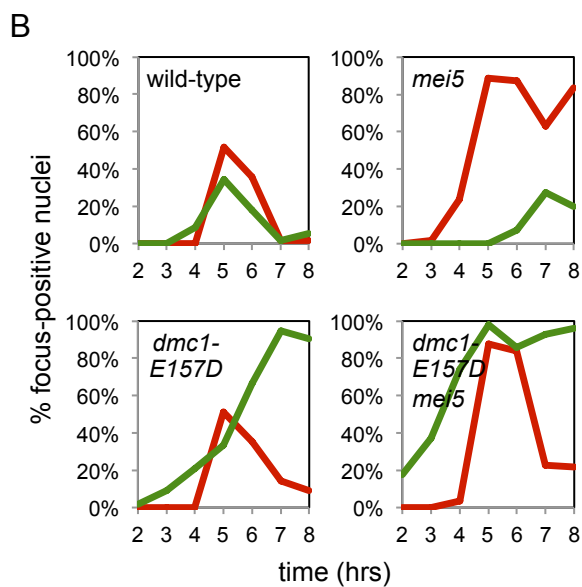
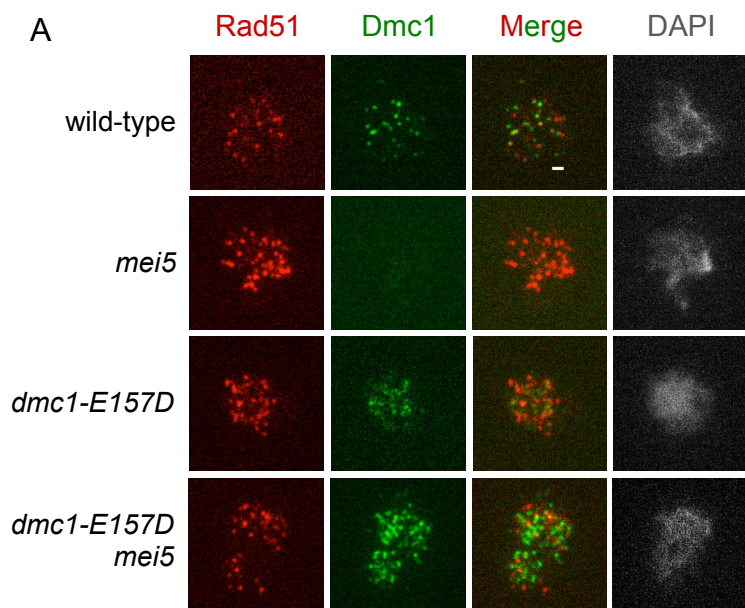
1212 Samples were collected 4 hours after induction of meiosis in liquid medium and immuno-stained for Dmc1
1213 and Hop2. Because Hop2 staining is Spo11 independent and specific for meiotic prophase, random
1214 prophase nuclei were selected on the basis of being Hop2 positive and then imaged for Dmc1 staining.
1215 50 nuclei were examined for each sample with 3 representative nuclei shown for each of the three strains
1216 examined. Images were generated by wide-field microscopy using the same camera settings for all
1217 strains. Strains used in this experiment in the order in which they appear in figure, top to bottom:
1218 DKB2524, DKB2523, and DKB6571.

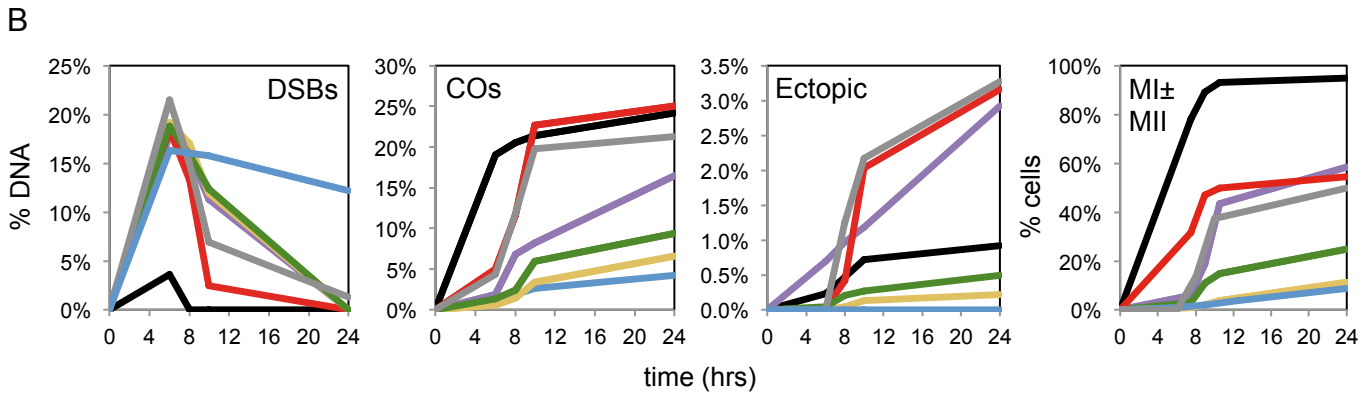
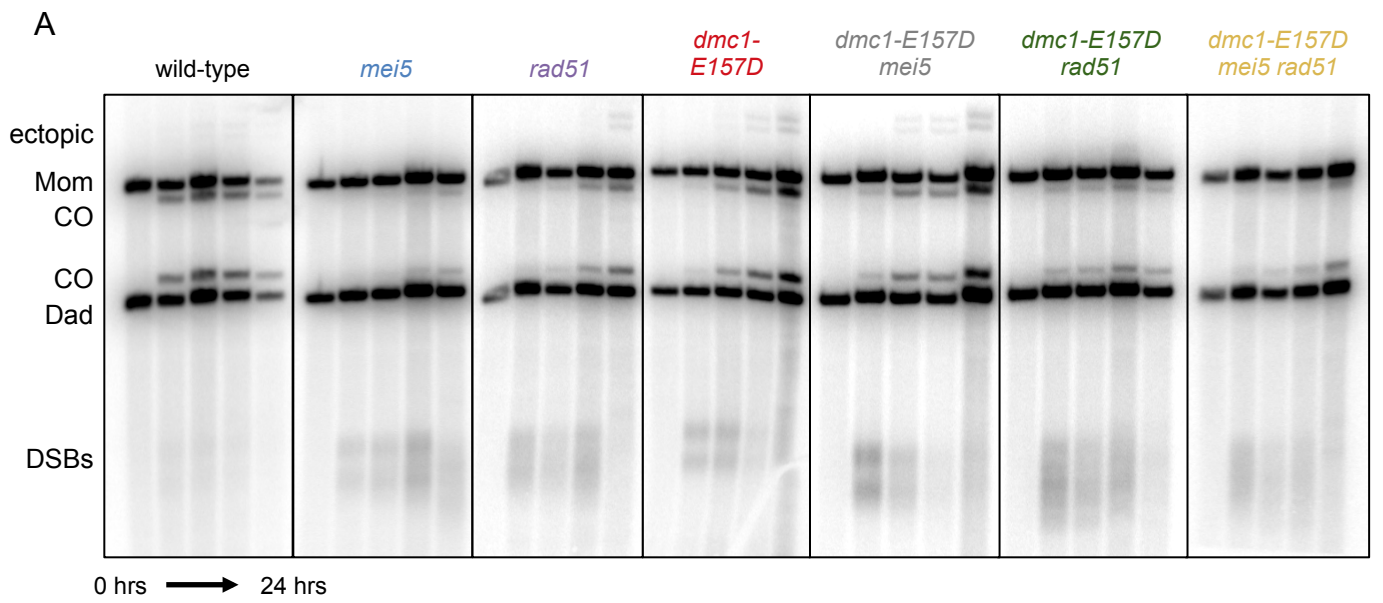
1219

1220 **Supplemental Table 1.** Yeast strains used in this study.

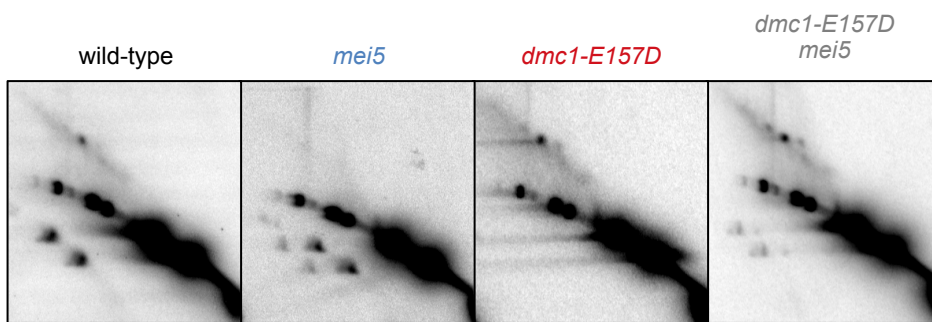
1221

| Strain | n (tetrads) | Spore viability (%) | p-value (z-score) |
|------------------------------|--------------------|----------------------------|--------------------------|
| wild-type | 153 | 98.4 | N.A. |
| <i>mei5</i> | no tetrads formed | N.A. | N.A. |
| <i>rad51</i> | 160 | 0.0 | N.A. |
| <i>rad51-II3A</i> | 76 | 82.9 | p < 0.01 |
| <i>rdh54</i> | 40 | 91.9 | p < 0.01 |
| <i>dmc1-E157D</i> | 215 | 57.6 | p < 0.01 |
| <i>dmc1-E157D mei5</i> | 253 | 50.3 | p < 0.01 |
| <i>dmc1-E157D sae3</i> | 39 | 57.0 | not significant |
| <i>dmc1-E157D rad51</i> | 136 | 0.74 | N.A. |
| <i>dmc1-E157D rad51-II3A</i> | 88 | 17.0 | p < 0.01 |
| <i>dmc1-E157D rdh54</i> | no tetrads formed | N.A. | N.A. |
| <i>dmc1-E157D mei5 rad51</i> | no tetrads formed | N.A. | N.A. |
| <i>DMC1/dmc1-E157D</i> | 160 | 85.6 | p < 0.01 |
| <i>DMC1/dmc1-E157D mei5"</i> | 160 | 58.8 | p < 0.01 |

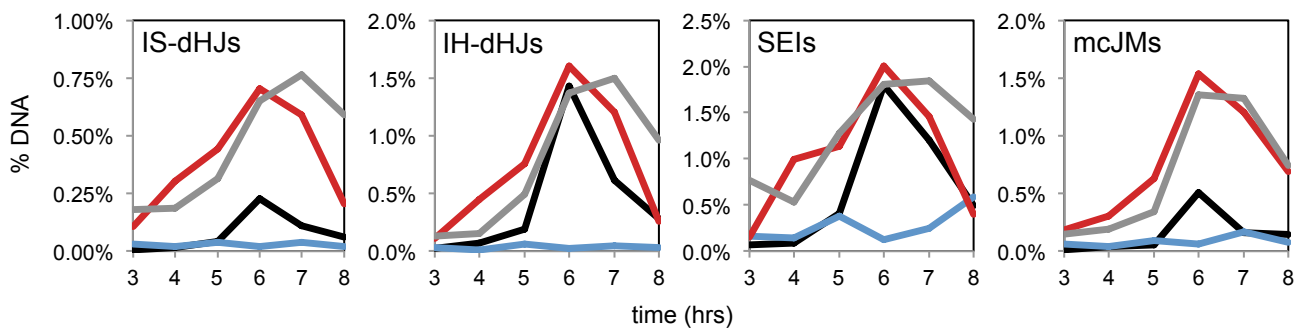




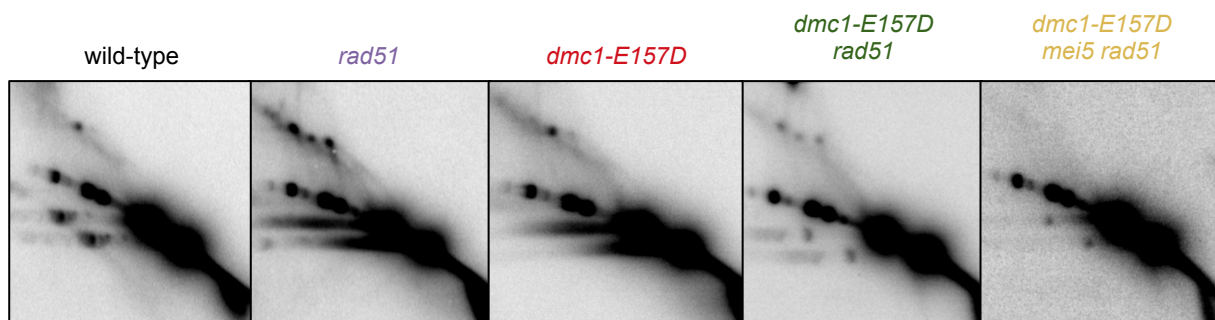
A



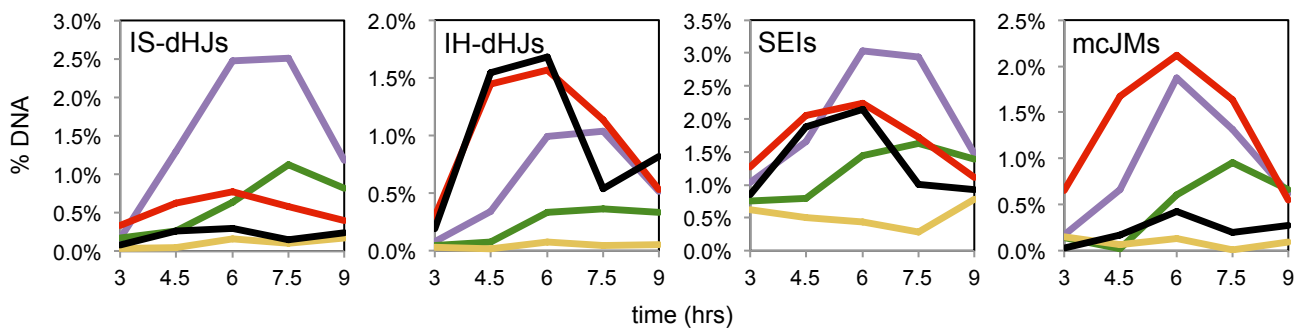
B

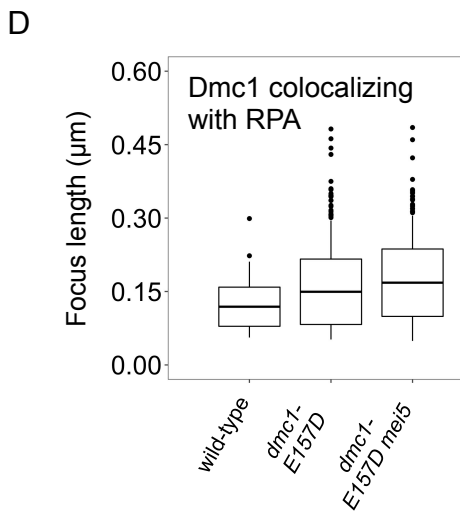
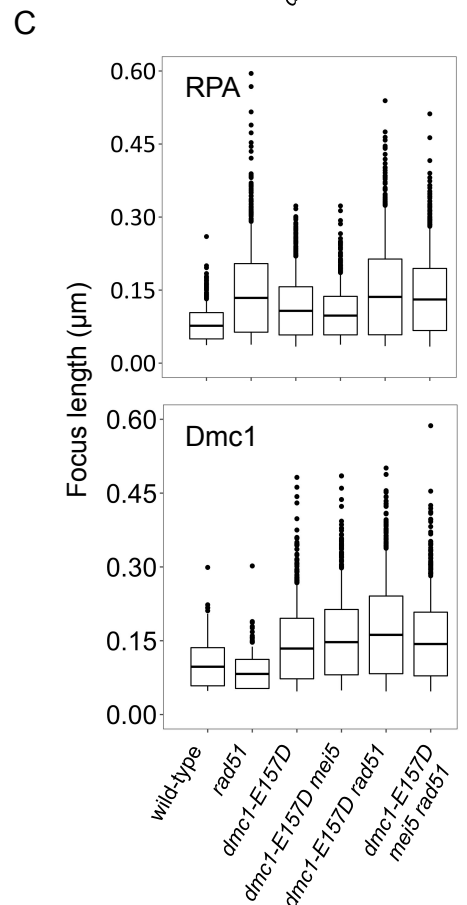
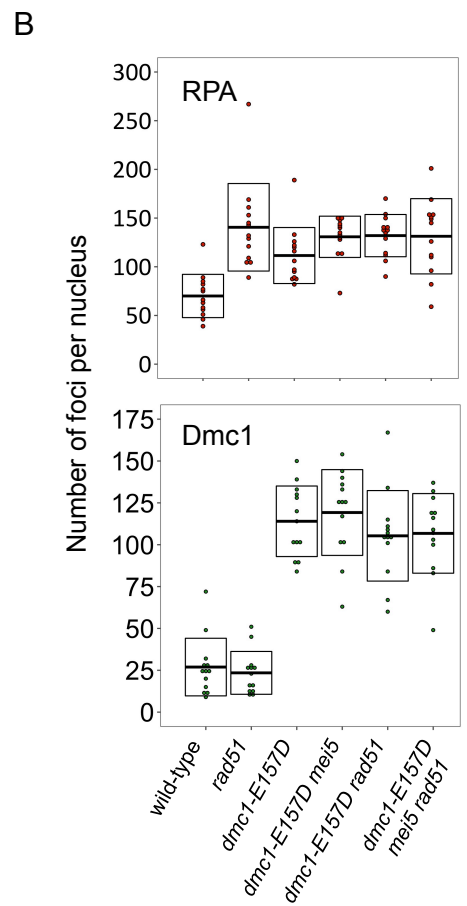
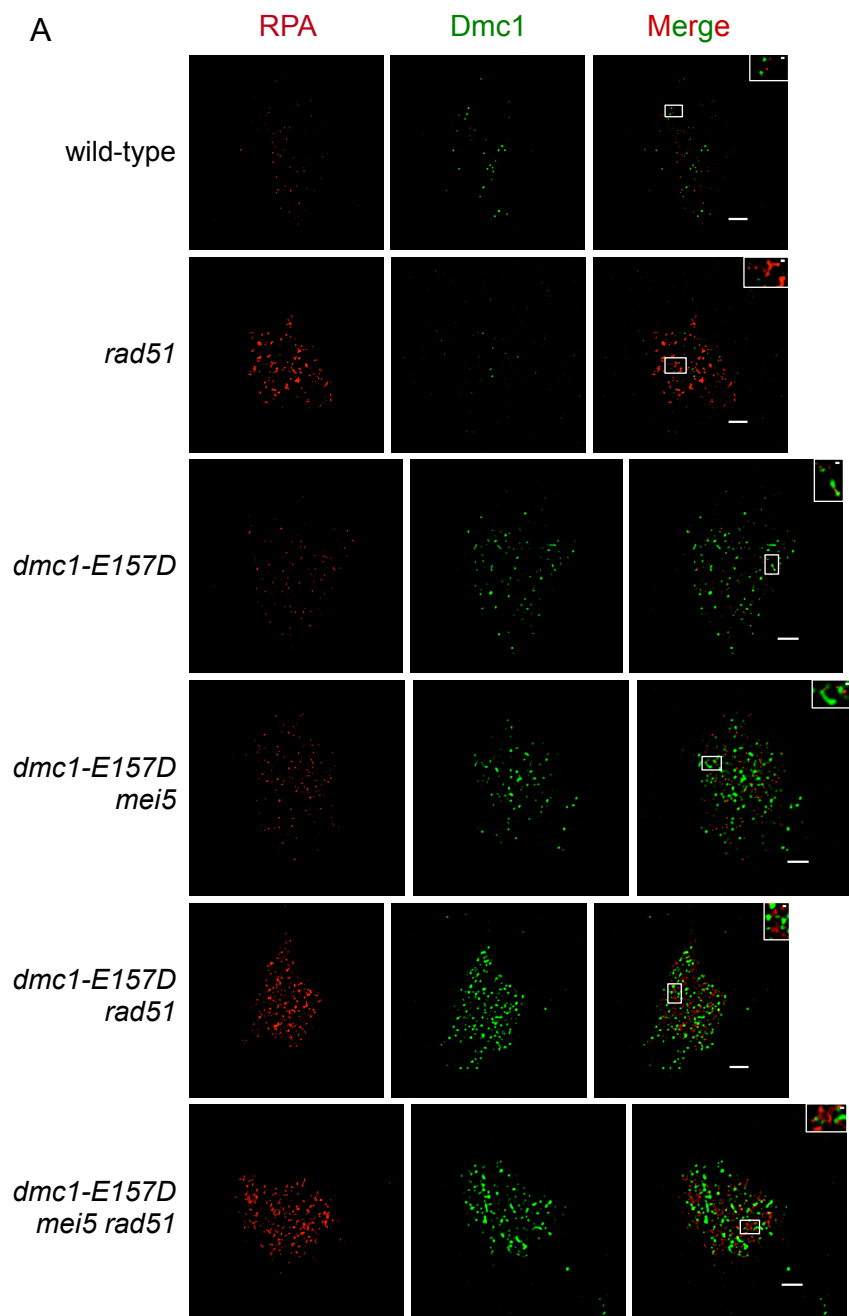


C

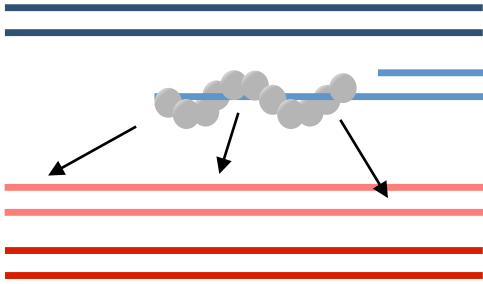


D

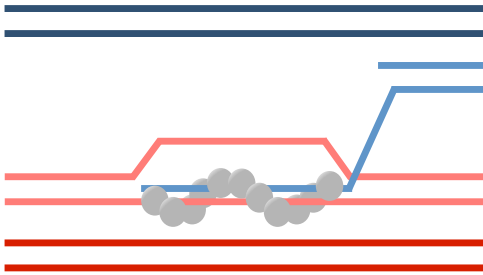




Short filaments

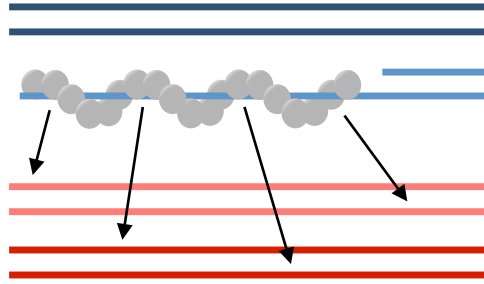


homology search within filament is limited

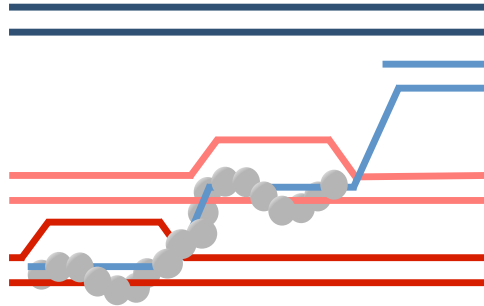


filament invades a single donor





Long filaments

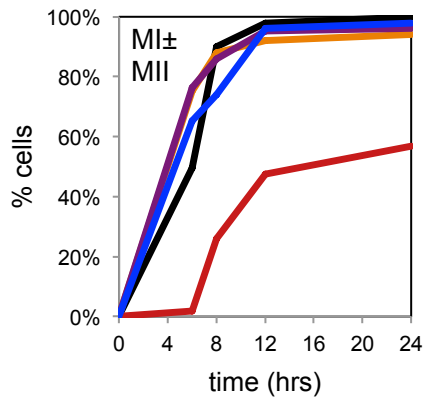


homology search within filament is wide-ranging



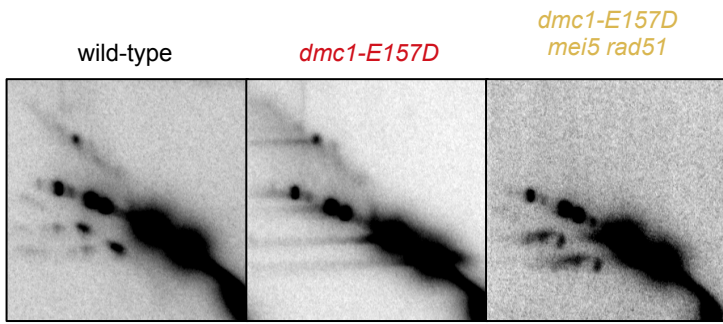
filament may invade multiple donors

| | Dmc1 6 hr | Control | Expression relative to wild-type |
|-------------------|---|---|----------------------------------|
| wild-type |  |  | N.A. |
| <i>dmc1-E157D</i> |  |  | 0.95 |

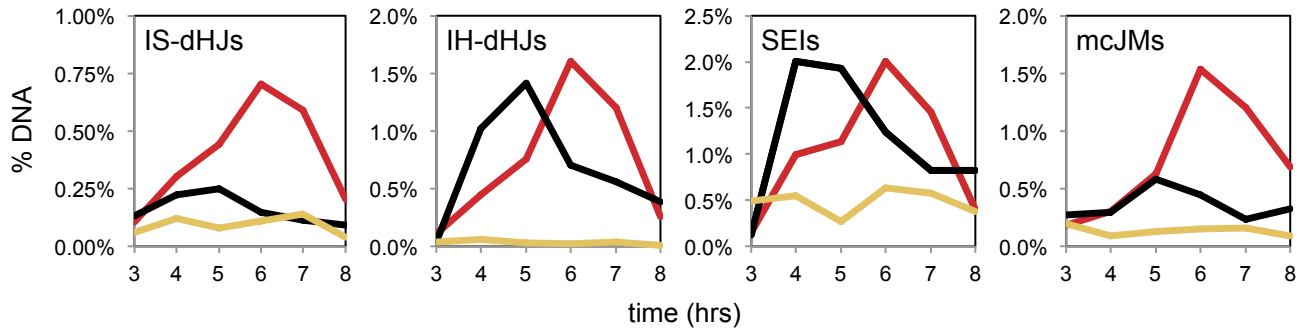


wild-type
spo11
dmc1-E157D
spo11 dmc1-E157D
spo11 dmc1-E157D mei5

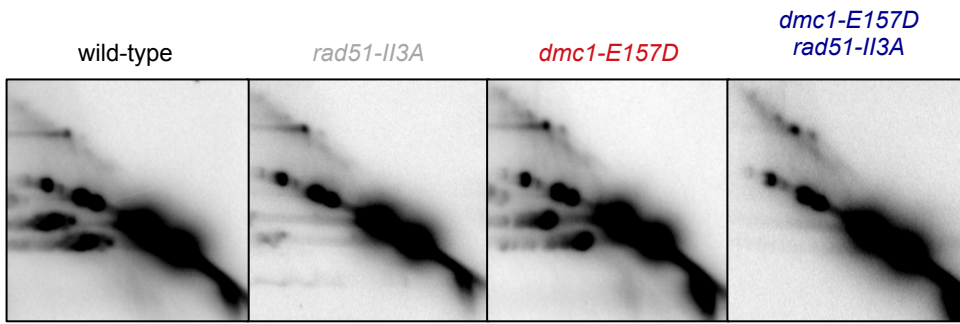
A



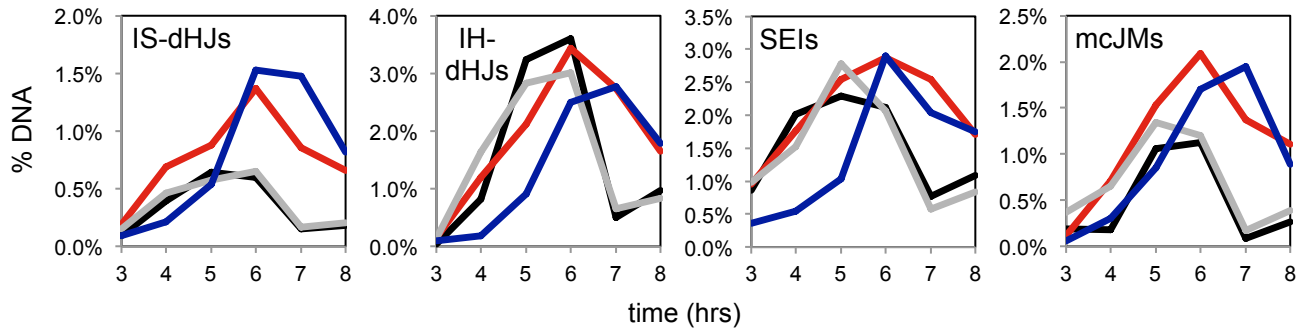
B

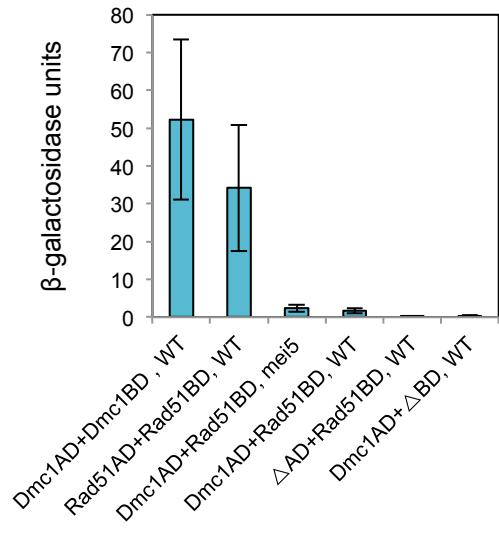
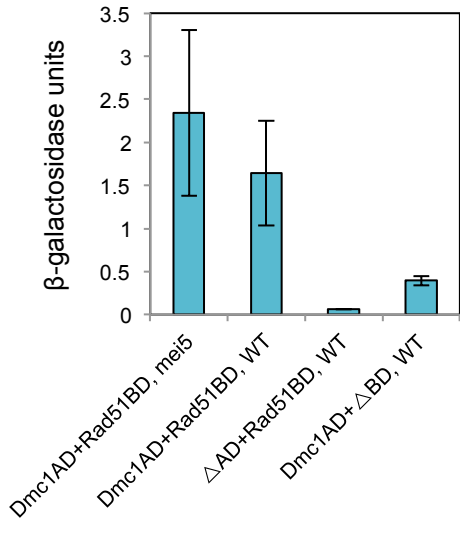


A



B

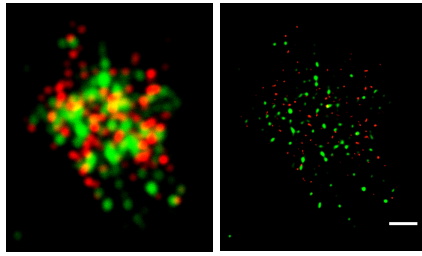


A**B**

A

confocal deconvolved
STED

dmc1-E157D
mei5



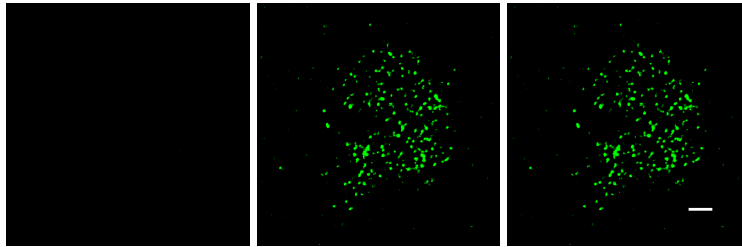
B

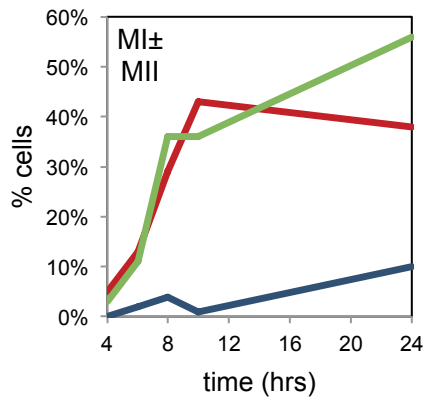
RPA

Dmc1

Merge

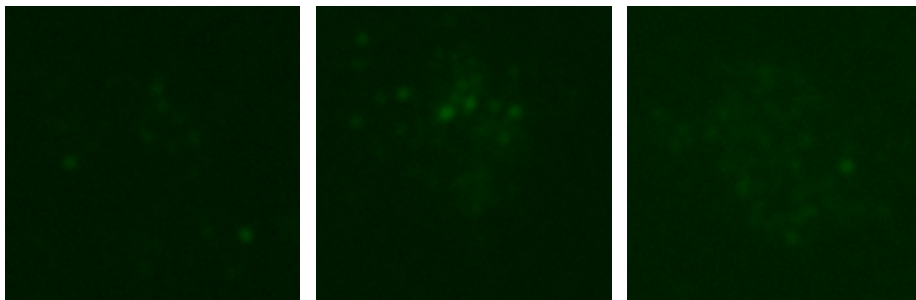
spo11 dmc1-
E157D



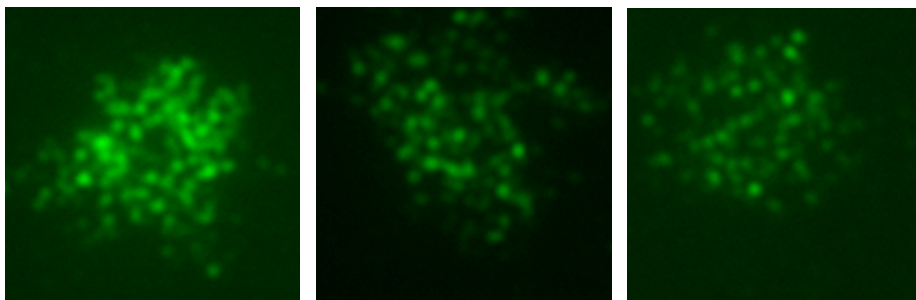


rdh54
dmc1-E157D
dmc1-E157D rdh54

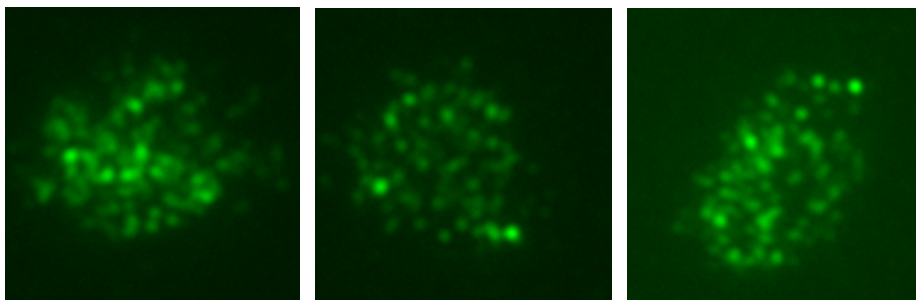
spo11



spo11 rdh54



spo11 rdh54 mei5



| Name | Strain | Genotype |
|------------------------------|---------|---|
| wild-type | DKB3698 | <i>ho::hisG^r, leu2::hisG^r, ura3(ΔSma-Pst)^r, HIS4::LEU2-(BamHI; +ori)/his4-X::LEU2-(NgoMIV; +ori)-URA3</i> |
| <i>dmc1-E157D</i> | DKB6342 | <i>lys2^r, ho::hisG/ho::LYS2, leu2::hisG, ura3^r, HIS4::LEU2-(BamHI; +ori)/his4-X::LEU2-(NgoMIV; +ori)-URA3, dmc1-E157D-natMX4^r</i> |
| <i>DMC1/dmc1-E157D</i> | DKB6619 | <i>lys2/LYS2, ho::hisG^r, leu2::hisG^r, ura3^r, HIS4::LEU2-(BamHI; +ori)^r, dmc1-E157D-natMX4/DMC1-WT</i> |
| <i>mei5</i> | DKB6320 | <i>ho::hisG^r, leu2::hisG^r, ura3^r, HIS4::LEU2-(BamHI; +ori)/his4-X::LEU2-(NgoMIV; +ori)-URA3, mei5::KANMX^r</i> |
| <i>rad51</i> | DKB3710 | <i>ho::hisG or LYS2^r, ura3^r, leu2::hisG^r, HIS4::LEU2-(BamHI; +ori)/his4X::LEU2-(NgoMIV; +ori)-URA3, rad51::hisG^r</i> |
| <i>rad51-Il3A</i> | DKB3689 | <i>ho::hisG^r, leu2::hisG^r, ura3(ΔSma-Pst)^r, HIS4-X::LEU2-(BamHI; +ori)-ura3/his4X::LEU2-(NgoMIV; +ori)-URA3, RAD51-R188A, K361A, K371A-KANMX6^r</i> |
| <i>rdh54</i> | DKB2526 | <i>ho::LYS2^r, lys2^r, leu2::hisG^r, his4-X::LEU2^r, trp1::hisG^r, tid1::LEU2^r</i> |
| <i>spo11</i> | DKB2123 | <i>ho::LYS2^r, lys2^r, leu2::hisG^r, ura3^r, his4-X/his4B, spo11::hisG-URA3-hisG^r</i> |
| <i>spo11</i> | DKB2524 | <i>ho::LYS2^r, lys2^r, leu2::hisG^r, trp1::hisG^r, ura3^r, his4X::LEU2^r, spo11::hisG-URA3-hisG^r</i> |
| <i>dmc1-E157D mei5</i> | DKB6299 | <i>ho::LYS2/ho::hisG, ura3^r, leu2::hisG^r, HIS4::LEU2-(BamHI; +ori)/his4-X::LEU2-(NgoMIV; +ori)-URA3, dmc1-E157D-natMX4^r, mei5::kanMX^r</i> |
| <i>dmc1-E157D mei5</i> | DKB6300 | <i>ho::LYS2/ho::hisG, ura3^r, leu2::hisG^r, HIS4::LEU2-(BamHI; +ori)/his4-X::LEU2-(NgoMIV; +ori)-URA3, dmc1-E157D-natMX4^r, mei5::kanMX^r</i> |
| <i>DMC1/dmc1-E157D mei5</i> | DKB6406 | <i>ho::hisG, leu2::hisG, ura3, his4-X::LEU2-(NgoMIV; +ori)-URA3/HIS4::LEU2-(BamHI; +ori), mei5::KanMX^r, dmc1-E157D-natMX4/DMC1-WT</i> |
| <i>DMC1/dmc1-E157D mei5</i> | DKB6407 | <i>ho::hisG, leu2::hisG, ura3, his4-X::LEU2-(NgoMIV; +ori)-URA3/HIS4::LEU2-(BamHI; +ori), mei5::KanMX^r, dmc1-E157D-natMX4/DMC1-WT</i> |
| <i>dmc1-E157D rad51</i> | DKB6393 | <i>lys2 or LYS2^r, ho::hisG or ho::LYS2^r, ura3^r, leu2::hisG^r, arg4-nsp/ARG4, his4-X::LEU2-(NgoMIV; +ori)-URA3/HIS4::LEU2-(BamHI; +ori), dmc1-E157D-natMX4^r, rad51::hisG^r</i> |
| <i>dmc1-E157D rad51-Il3A</i> | DKB6400 | <i>ho::hisG^r, leu2::hisG^r, ura3^r, HIS4::LEU2-(BamHI; +ori)/his4-X::LEU2-(NgoMIV; +ori)-URA, RAD51-R188A, K361A, K371A-KANMX6^r, dmc1-E157D-natMX4^r</i> |
| <i>dmc1-E157D rdh54</i> | DKB6583 | <i>ho::LYS2^r, lys2^r, leu2::hisG^r, his4-X::LEU2^r, TRP1/trp1::hisG, tid1::LEU2^r, dmc1-E157D-natMX4^r</i> |
| <i>dmc1-E157D sae3</i> | DKB6539 | <i>lys2^r, ho::LYS2^r, leu2 or LEU2^r, ura3^r, HIS4::LEU2-(BamHI; +ori)/his4-X::LEU2-(NgoMIV; +ori)-URA3, dmc1-E157D-natMX4^r, sae3::hisG-URA3-hisG^r</i> |
| <i>dmc1-E157D sae3</i> | DKB6540 | <i>lys2^r, ho::LYS2^r, leu2 or LEU2^r, ura3^r, HIS4::LEU2-(BamHI; +ori)/his4-X::LEU2-(NgoMIV; +ori)-URA3, dmc1-E157D-natMX4^r, sae3::hisG-URA3-hisG^r</i> |
| <i>spo11 dmc1-E157D</i> | DKB6419 | <i>ho::hisG or ho::LYS2/ho::hisG, LYS2 or lys2/lys2, leu2::hisG^r, ura3^r, his4-X::LEU2-(NgoMIV; +ori)-URA3/HIS4::LEU2-(BamHI; +ori), dmc1-E157D-natMX4^r, spo11::hisG-URA3-hisG^r</i> |
| <i>spo11 rdh54</i> | DKB2523 | <i>ho::LYS2^r, lys2^r, ura3^r, leu2::hisG^r, his4-X::LEU2^r, trp1::hisG^r, tid1::LEU2^r, spo11::hisG-URA3-hisG^r</i> |
| <i>dmc1-E157D mei5 rad51</i> | DKB6412 | <i>lys2 or LYS2^r, ho::hisG or ho::LYS2^r, ura3^r, leu2::hisG^r, arg4-nsp or ARG4/ARG4, HIS4::LEU2-(BamHI; +ori)/his4-X::LEU2-(NgoMIV; +ori), rad51::hisG^r, dmc1-E157D-natMX4^r, mei5::KANMX^r</i> |
| <i>dmc1-E157D mei5 rad51</i> | DKB6413 | <i>lys2 or LYS2^r, ho::hisG or ho::LYS2^r, ura3^r, leu2::hisG^r, arg4-nsp/ARG4, HIS4::LEU2-(BamHI; +ori)/his4-X::LEU2-(NgoMIV; +ori), rad51::hisG^r, dmc1-E157D-natMX4^r, mei5::KANMX^r</i> |
| <i>spo11 dmc1-E157D mei5</i> | DKB6425 | <i>ho::hisG or ho::LYS2^r, lys2 or LYS2^r, leu2::hisG^r, ura3^r, HIS4::LEU2-(BamHI; +ori)/his4-X::LEU2-(NgoMIV; +ori)-URA3, dmc1-E157D-natMX4^r, spo11::hisG-URA3-hisG^r, mei5::KANMX^r</i> |
| <i>spo11 mei5 rdh54</i> | DKB6571 | <i>ho::LYS2^r, lys2^r, ura3^r, leu2::hisG^r, his4-X::LEU2^r, trp1::hisG^r, tid1::LEU2^r, spo11::hisG-URA3-hisG^r, mei5::KANMX^r</i> |
| two-hybrid strain | DKB6501 | <i>lys2^r, ho::LYS2^r, URA3^r, leu2:hisG^r, his4-X/HIS4, trp1::hisG^r, arg4-nsp or ARG4^r, dmc1::ARG4^r, rad51::hisG^r, ndt80::kanMX^r, LexA(op)-lacZ::URA3^r +pNRB729 +pNRB271</i> |
| two-hybrid strain | DKB6503 | <i>lys2^r, ho::LYS2^r, URA3^r, leu2:hisG^r, his4-X/HIS4, trp1::hisG^r, arg4-nsp or ARG4^r, dmc1::ARG4^r, rad51::hisG^r, ndt80::kanMX^r, LexA(op)-lacZ::URA3^r +pNRB727 +pNRB688</i> |
| two-hybrid strain | DKB6508 | <i>lys2^r, ho::LYS2^r, URA3^r, leu2:hisG^r, HIS4/his4-X, trp1::hisG^r, arg4-nsp or ARG4^r, dmc1::ARG4^r, mei5Δ::kanMX^r, rad51::hisG^r, ndt80::kanMX^r, LexA(op)-lacZ::URA3^r +pNRB727 +pNRB271</i> |
| two-hybrid strain | DKB6509 | <i>lys2^r, ho::LYS2^r, URA3^r, leu2:hisG^r, his4-X/HIS4, trp1::hisG^r, arg4-nsp or ARG4^r, dmc1::ARG4^r, rad51::hisG^r, ndt80::kanMX^r, LexA(op)-lacZ::URA3^r +pNRB727 +pNRB271</i> |
| two-hybrid strain | DKB6513 | <i>lys2^r, ho::LYS2^r, URA3^r, leu2:hisG^r, his4-X/HIS4, trp1::hisG^r, arg4-nsp or ARG4^r, dmc1::ARG4^r, rad51::hisG^r, ndt80::kanMX^r, LexA(op)-lacZ::URA3^r +pNRB728 +pNRB271</i> |
| two-hybrid strain | DKB6515 | <i>lys2^r, ho::LYS2^r, URA3^r, leu2:hisG^r, his4-X/HIS4, trp1::hisG^r, arg4-nsp or ARG4^r, dmc1::ARG4^r, rad51::hisG^r, ndt80::kanMX^r, LexA(op)-lacZ::URA3^r +pNRB727 +pNRB267</i> |